Dynamic Power Cable Optimized Configurations for Lazy Wave Riser Systems

Auteur : Guzman Guzman, Edwin Eduardo
Promoteur(s) : Rigo, Philippe
Faculté : Faculté des Sciences appliquées
Diplôme : Master : ingénieur civil mécanicien, à finalité spécialisée en "Advanced Ship Design"
Année académique : 2023-2024
URI/URL : http://hdl.handle.net/2268.2/22256

Dynamic Power Cable Optimized Configurations for Lazy Wave Riser Systems

Submitted on 27 August, 2024

by

GUZMÁN Eduardo
Street No. Calle Bretón de los Herreros, 32
ZIP Town: 28003
email address: eduardo.guzman@alumnos.upm.es
Student ID No. S221718

Supervisors:

Tomás López Olocco
tomas.lopez@upm.es
UPM

Santiago de Guzmán
sguzman@seaplace.es
Seaplace

First Reviewer:

Giles Barkley
giles.barkley@solent.ac.uk
Room no. RM403
Southampton
United Kingdom

Second Reviewer:

Gustavo Fabián Acosta
gustavo.acosta@alumnos.upm.es
Av. de la Memoria, 4
Madrid
Spain

EMship+ Advanced Design

MASTER THESIS

[This page is intentionally left blank]

Contents

List of Figures

List of Tables

[This page is intentionally left blank]

DECLARATION OF AUTHORSHIP

I, **Eduardo Guzmán** declare that this thesis and the work presented in it are my own and have been generated by me as the result of my own original research.

Where I have consulted the published work of others, this is always clearly attributed.

Where I have quoted from the work of others, the source is always given. With the exception of such quotations, this thesis is entirely my own work.

I have acknowledged all the main sources of help.

Where the thesis is based on work done by myself jointly with others, I have made it clear exactly what was done by others and what I have contributed myself.

This thesis contains no material that has been submitted previously, in whole or in part, for the award of any other academic degree or diploma.

I cede copyright of the thesis in favour of the Polytechnic University of Madrid.

Date: August 25th, 2024

Signature: 

[This page is intentionally left blank]

ACKNOWLEDGEMENTS

I express my deepest gratitude to my supervisors, Dr. Tomas Lopez Olocco, and Santiago de Guzmán, M.Sc. for their continuous support and guidance throughout my research. I also want to thank my committee members, Dr. Giles Barkley and Gustavo Acosta, M.Sc., for their valuable feedback and suggestions. I would like to express my gratitude to alumni friends, Jonathan Arellano and Priscilla Loor, for their invaluable advice and friendship.

I am deeply grateful to my family for their unwavering support and encouragement.

ABSTRACT

The rapid development of floating offshore wind energy requires advanced solutions for power transmission, particularly in the context of dynamic environments such as array and export cables. This thesis investigates optimized configurations for dynamic power cables within lazy wave riser systems, with the aim of enhancing performance and reliability while reducing the length of the cable. The study begins with a comprehensive review of offshore wind energy, comparing offshore and onshore wind farms, and detailing the design standards and criteria relevant to cable design.

A systematic method is used to examine and improve the configuration of dynamic power cables. This includes conducting static analyzes, dynamic evaluations, and fatigue studies taking into account the environmental conditions of the site. A quasi-static model is created to study the cable, focusing on the lazy wave design. The cable is segmented into three parts: the drag section, the buoyancy section, and the sagging section. Subsequently, a nonlinear equation system is resolved for predetermined locations of the hang-off point on the floater and the anchor point of the cable.

Subsequently, various lazy wave configurations are examined in Orcaflex, and as the stress factors methods are used to evaluate stress, every configuration is analyzed for curvature and effective tension in order to reduce the stress; the first configuration places the top of the buoyancy section at around one-fourth of the water depth, the second configuration positions the top of the buoyancy section at about one-half of the water depth, and the third configuration locates the buoyancy section's top at roughly three-fourths of the water depth. For every configuration, an optimization is carried out; the tension at the hang-off point is minimized, the curvature in the sagging section is decreased to a specific reference value necessary to reduce motion at the TDP, the curvature in the remainder of the cable is also reduced, and the overall length of the cable is minimized as well.

The environmental conditions of the site are represented by 20 short-term sea states, fatigue damage is determined by examining the cable response over a 30-minute dynamic simulation for each sea condition. The critical location of the lazy wave design is found in the HOP. A design that uses a shorter cable length and maintains a lifespan that exceeds 32 years at this location is considered as good candidate.

This thesis ends with the proposal of a new configuration for the dynamic power cable, summarizing key findings that can improve performance. Upon a thorough understanding of the system, several topics are identified for future research.

1. INTRODUCTION

The use of renewable energies by humans can be traced back to ancient times. One of the first examples is the use of water or windmills to transform potential energy into mechanical movement, which was used to grind grains [14]. Since then, technology has evolved considerably. Currently, there are numerous options for energy converters on the market, and the selection of these options is influenced by the specific needs and the type of energy being transformed.

The use of renewable energies is becoming one of the favorite sources of energy in the global community, since it is almost an infinite source of energy. In addition, it has a small negative impact on the environment as a result of its lowest carbon footprint compared to other sources of energy [13]. Recent innovation allowed to reduce the **levelized cost of energy (LCOE)**, making it more attractive to new investments.

Offshore wind energy has emerged as a crucial component of the global renewable energy portfolio due to its numerous advantages. One of the primary benefits is the abundance and consistency of the wind resources available offshore. Unlike onshore sites, where buildings and trees can obstruct wind flow, offshore locations benefit from stronger and more consistent wind speeds. This results in a higher energy yield, making offshore wind farms more efficient. Furthermore, the open sea provides ample space for large-scale energy production, allowing for the installation of larger turbines and expansive wind farm arrays.

Strategic placement of wind turbines closer to densely populated coastal regions reduces transmission losses and improves energy delivery efficiency [10]. The environmental benefits of offshore wind energy are substantial as it significantly reduces greenhouse gas emissions and decreases the dependence on fossil fuels.

Continuous advancements in offshore wind technology have improved efficiency and reduced costs. Technological innovations such as larger turbines and floating platforms have expanded the potential for offshore wind energy, even in deeper waters. These technological advances, along with improved installation and maintenance techniques, increase the overall viability of offshore wind projects, making them a promising solution for sustainable energy production.

1.1. State of the art

The European Union (EU) has set a target of installing 200 gigawatts (GW) of new wind power capacity between 2024 and 2030 (Fig. 1), which equates to an average of 29 [GW] per year. In order to meet its 2030 climate and energy targets, the EU must now build an additional 33 [GW] per year on average [11].

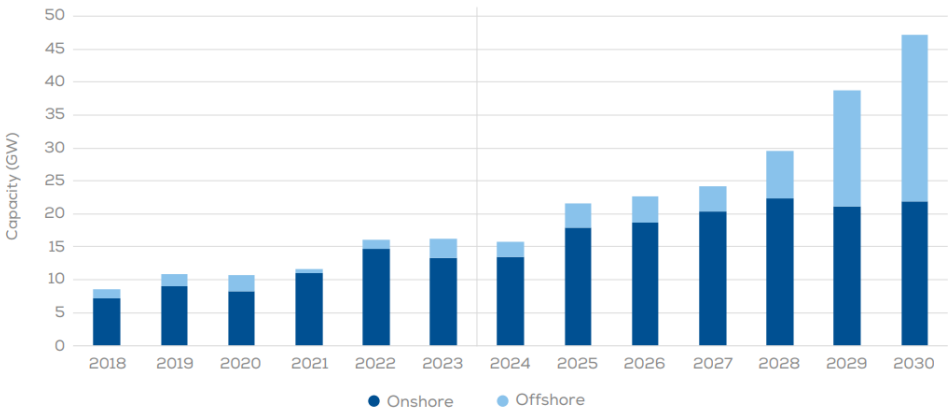

Figure 1: Annual wind power installation [11].

1.1.1. Offshore wind farms

Several offshore wind farms are currently operational around the world, demonstrating the viability and benefits of offshore wind energy. For instance, Europe has seen a substantial increase in offshore wind capacity, with countries such as the UK, Germany, and Denmark leading the way. In 2023, Europe had more than 28 [GW] of installed offshore wind capacity [11], with numerous projects under development (Fig. 2).

Spain also leads Europe in wind energy, but remains new to the commercial offshore wind sector. The Spanish government recently wrapped up consultations for its first Offshore Wind Strategy, aiming to create the nation's initial commercial offshore wind farms. This sets an ambitious goal of achieving 3 [GW] of offshore wind capacity by 2030, supported by at least 200 € million for research and development in offshore wind technologies [27]. Although Spain currently has 27 [GW] of wind energy capacity, mainly from onshore sources, the Strategy marks a significant move toward offshore wind expansion.

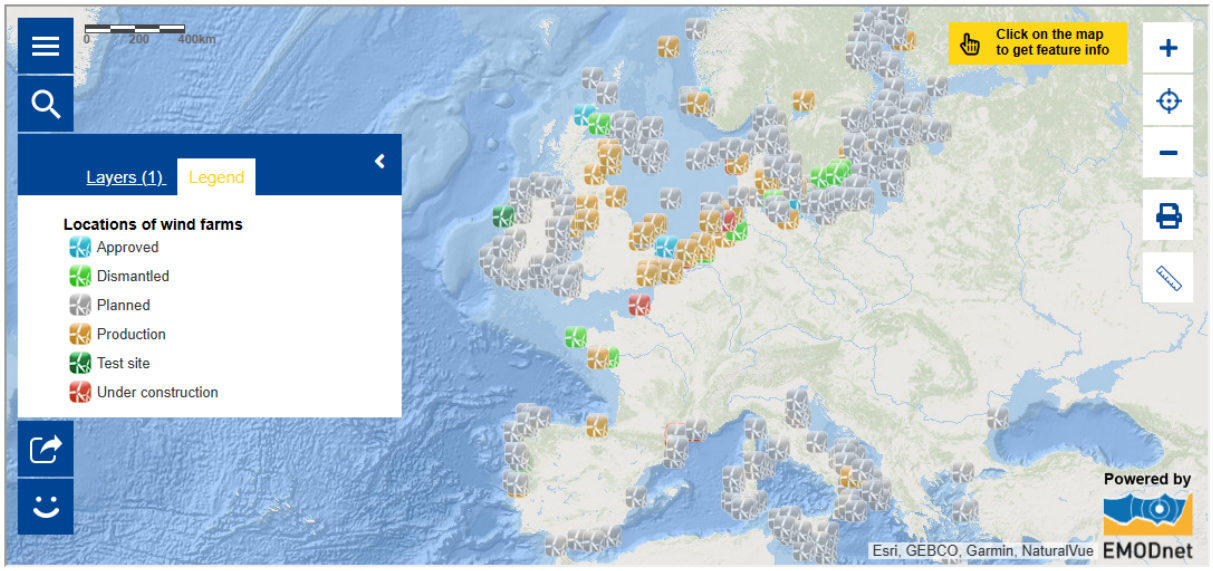

Figure 2: European wind farm locations [23].

The buffer shown in (Fig. 3) extends 100 km from the coastline. It is noticeable that in Galicia, the average annual wind speed is approximately 10 m/s, and there are areas where the bathymetry is less than 200 meters. This makes the location a promising candidate for floating offshore wind turbines.

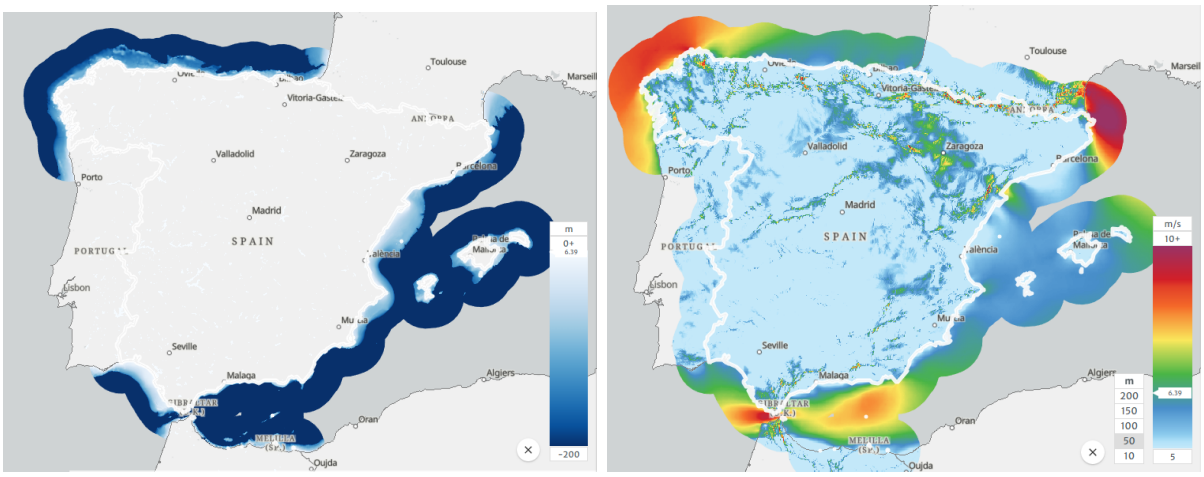

(a) Bathymetry. **(b)** Mean annual wind speed at 50 m.

Figure 3: Underwater topography and wind speeds along the Spanish coastline [2].

1.1.2. Offshore platforms

Offshore wind turbines are mounted on platforms that can be fixed to the seabed or floating. Fixed platforms are used in shallow waters , while floating platforms (Fig. 4) are suitable for depth waters, normally greater than 60 [m]. Floating wind turbines are an emerging technology that allows wind farms to be installed in deeper waters, unlocking

significant potential for wind energy generation in previously inaccessible areas.

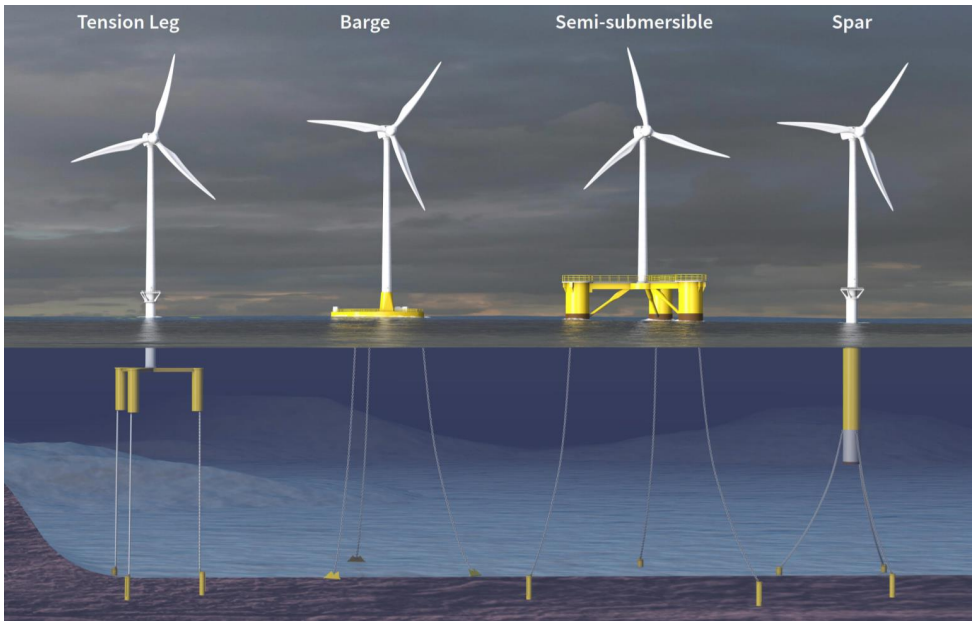

Figure 4: Floating offshore wind turbines [15].

Tension Leg Platform (TLP)

A TLP is an offshore floating structure tethered to the seabed through vertical tendons that are kept in continuous tension. The platform itself is buoyant, staying afloat at the surface, while the tendons ensure stability by counteracting buoyant forces.

TLPs are used in various applications, such as deep-water offshore wind farms. They are especially effective in regions where deep water prevents the use of conventional fixed foundations. Due to their inherent stability, TLPs are well suited for locations with moderate to strong wave and wind conditions.

The TLP offers excellent vertical stability with minimal vertical motion (heave) due to the tension in the mooring tendons. This makes it perfect for maintaining steady turbine operations and minimizing dynamic forces on the wind turbine. Although the TLP does exhibit some horizontal motion (surge and sway), these movements are relatively minor compared to other floating platforms. The reduced vertical and controlled horizontal motion enhances the performance and durability of offshore wind turbines.

Barge Platform

A barge platform is a buoyant structure with a flat bottom, commonly used in shallow to moderate water depths. The platform is designed simply, relying on buoyancy for its stability in the water. This straightforward design is often more economical compared to other floating alternatives.

Barge platforms are deployed in offshore wind projects where water depths are relatively shallow, generally up to roughly 30 meters. These platforms are often employed in the early stages of a project or in locations with less severe environmental conditions.

Barge platforms are prone to significant vertical (heave) and horizontal (surge and sway) motions due to their large surface area and shallow draft. Such dynamics can cause substantial loading on the wind turbine and its systems. The significant movement necessitates robust design considerations to manage associated stresses and ensure reliable turbine operation. The increased mobility makes barge platforms less suitable for harsh marine conditions or deeper waters.

Semi-Submersible Platform

A semi-submersible platform is characterized as a floating structure supported by submerged pontoons linked by vertical columns. The submersion of the pontoons helps distribute buoyancy forces and ensures stability.

Semi-submersible platforms are employed in offshore wind farms at various water depths, ranging from shallow to deep waters, with usual depths reaching up to around 200 meters. These platforms are ideal for locations with changing environmental conditions, including moderate to high wave and wind intensity.

The design of semi-submersibles enhances their stability, resulting in minimal vertical motion (heave). This feature helps to ensure the reliable functioning of offshore wind turbines. However, some horizontal movement is noted, though less than that of barge platforms. The stability provided by semi-submersibles reduces the dynamic forces on wind turbines, making them a versatile and reliable choice for various offshore scenarios.

Spar Platform

A spar platform is characterized as a deep-draft floating structure with an elongated cylindrical hull, anchored to the seabed with mooring lines. The hull is submerged to a depth below the water's surface, achieving stability by combining its buoyant properties with the anchoring system.

Spar platforms are used in marine environments of significant depths. They are suitable for areas where other floating platforms may lack stability. Spar platforms are ideal for deep-water wind farms, where maintaining a stable position is crucial due to strong waves and winds.

Spar platforms exhibit exceptional stability with minimal vertical and horizontal displacement, thanks to their deep draft and anchoring system. The design reduces both heave and sway, making it an optimal choice for maintaining consistent turbine operation in deep-water environments. The decrease in motion ensures that the dynamic forces acting on the wind turbine are minimal, thereby enhancing the overall reliability and performance of the offshore wind farm.

1.1.3. Electrical system design

The electrical system of an offshore wind farm includes various components such as turbines, substations, and power cables (Fig. 5). The design must ensure reliable transmission of electricity from the turbines to the shore while minimizing losses and accommodating the dynamic marine environment. Advanced electrical systems, including **high voltage direct current (HVDC)** technology, are increasingly being used to improve efficiency and reduce losses over long distances.

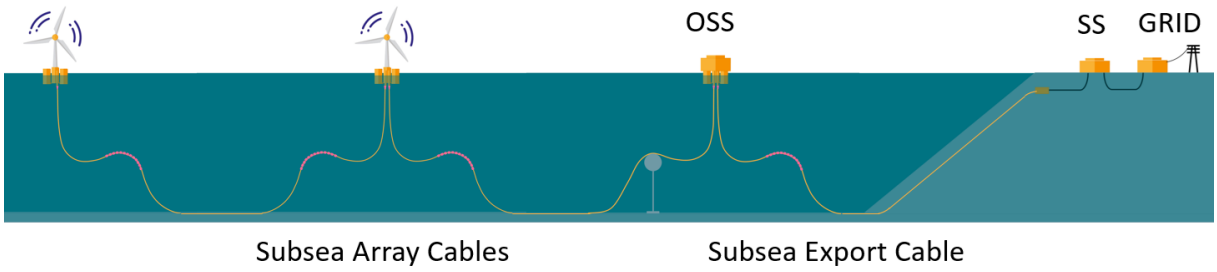

Figure 5: Typical configuration of an electrical system [15].

1.2. Problem statement

Despite its benefits, the offshore wind energy sector faces several challenges, particularly in the design and optimization of the infrastructure, because it is a relatively new field. A critical component in this setup is the **dynamic power cable (DPC)**, which must be meticulously engineered to withstand various environmental loads while maintaining optimal performance. When designing the DPC, there is a lack of information on the procedures, and it is not easy to find a methodology that covers all the design process of this system.

An efficient tool to perform such an analysis is crucial in early design stages. Seaplace, an offshore consulting firm that provides customized solutions for the offshore wind energy sector, sees the need for a methodology to clearly address this problem. A request has been

issued to propose a simplified methodology for designing and analyzing the configuration of the dynamic power cable, one of the most critical components of an offshore **floating wind turbine (FWT)**. The importance of a well-established methodology to properly design this component is significant, as any malfunction or failure can have an economic impact on the wind farm.

In contrast to onshore wind energy generators, the $O\&M$ strategy for offshore wind farms operates on a scheduled basis for maintenance activities, which considers factors such as weather conditions and specialized vessel availability, sometime although the resources are available, the site cannot be accessed. When a DPC flails, it is not just the replacement cost that must be taken into account, the loss of production and the expenses of arranging an unscheduled campaign to replace the component must also be included.

1.3. Objectives of the thesis

The primary objective of this thesis is to develop a simplified methodology to design and optimize DPC systems in offshore floating wind energy projects, with a special focus on the lazy wave configuration. Using this methodology, a preliminary design of the dynamic cable can be developed in the early stages of the design process. The design of the cable involves carefully optimizing both the length of the dynamic cable and the floaters distribution, then performing fatigue analysis to confirm that the optimized cable meets the required design life criteria.

1.3.1. Specific objectives

To effectively analyze a DPC, specific information is often required that may not be readily available or may need additional research to define. To address these challenges, the following specific objectives are identified:

- Conduct extensive research on the state of the art in umbilical cable design, define the cable properties to be used in this study, and determine the methods for damage evaluation.
- Establish the environmental loads necessary to perform static, dynamic and fatigue analyzes.
- Develop an analytical approach tailored for the conceptual design of the cable, to determine the stress distribution and to estimate the fatigue life.
- Provide a methodology for optimizing the configuration of umbilical cables.
- Propose a configuration for the dynamic power cable that minimizes capital investment while maintaining an acceptable fatigue life.

1.4. Structure of the Thesis

Introduction (Chapter 1)
This chapter gives a brief introduction of the floating offshore wind energy sector, and highlights the importance of the DPC in the electric system. The problem statement is outlined and the objectives required to develop a solution are clearly defined.

Theoretical background (Chapter 2)
This chapter gives additional information about the standards for the DPCs, provides relevant information for the cost estimation, and finally describe an optimization algorithm used in Chapter 5.

Methodology (Chapter 3)
Chapter 3 plays a key role in comprehending the following sections. It provides essential details about the cable, outlines the load conditions and sea states, presents the optimization method utilized in Chapter 5, and finally explains how fatigue is assessed using the stress factors method.

Quasi-static cable model (Chapter 4)
Chapter 4 provides a comprehensive explanation of the quasi-static model, beginning with the derivation of the elastic catenary equations and concluding with an assessment of the cable's fatigue life.

Power cable design (Chapter 5)
Chapter 5 utilizes OrcaFlex to examine the DPC lazy wave configuration, followed by an optimization process to improve the DPC setup. Subsequently, fatigue life is evaluated using the stress factor method and the results are analyzed to suggest a novel lazy wave configuration.

Conclusions (Chapter 6)
The key findings from Chapters 3-5 are outlined here, in line with the specific objectives. In addition, a set of activities is suggested as future work for those interested in continuing this research.

2. THEORETICAL BACKGROUND

2.1. Design standards and criteria

2.1.1. Relevant standards for cable design

The design of dynamic power cables for offshore applications must adhere to international standards and guidelines. These standards ensure that cables can withstand harsh marine conditions and maintain their structural integrity throughout their operational life. Standards such as IEC 60287 for electrical cable design and DNV GL standards for subsea power cables provide comprehensive guidelines for designing reliable and durable cables.

New electrical standard (december 2019)

- IEC 63026 Submarine power cables with extruded insulation and their accessories for rated voltages from 6 kV (Um = 7.2 kV) to 60 kV (Um = 72.5 kV) - Test methods and requirements.

Major electrical standards

- IEC 60228 - Conductors for insulated cables.
- IEC 60502-2 - Power cables with extruded insulation and their accessories for rated voltages - Part 2: Cables for rated voltages from 6 kV (Um = 7.2 kV) to 30 kV (Um = 36 kV).
- IEC 60840 - Power cables with extruded insulation and their accessories for rated voltages above 30 kV (Um = 36 kV) up to 150 kV (Um = 170 kV) - Test methods and requirements
- IEC 61892-4 Edition 2.0 2019-04: Mobile and fixed offshore units - Electrical installations - Part 4: Cables

Major optical standards

- ITU-T G.652 - Characteristics of singlemode optical fiber and cable
- ITU-T G.651.1 - Characteristics of a 50/125 µm multimode graded index optical fiber cable for the optical access network

Other standards / recommendations

- ISO 13628-5 - Petroleum and natural gas industries - Design and operation of subsea production systems - Part 5: Subsea umbilicals
- Cigré TB 490 - Recommendations for the testing of long-distance submarine cables
- Cigré TB 623 - Recommendations for mechanical testing of submarine cables.

- Cigré TB 722 - Recommendations for additional testing of submarine cables.

Historical Standards / Recommendations

- Cigré ELECTRA 189 - Recommendations for the testing of long length submarine cables.
- Cigre ELECTRA 171 - Recommendations for mechanical testing of submarine cables.
- Cigre ELECTRA 77 - Recommendations for mechanical testing of submarine cables.
- DNVGL-RP-0360 - Shallow water submarine power cables
- DNVGL-RP-F401 - Power cables in submarine applications
- DNVGL-ST-0359 - Subsea power cables for wind turbines

2.1.2. Criteria for performance and safety

Performance criteria include the ability of the cable to carry the required electrical load without excessive losses. Safety criteria involve the mechanical strength of the cable, its resistance to corrosion, and its ability to operate under various environmental conditions. Ensuring compliance with these criteria is essential for the long-term reliability and safety of offshore wind farms.

2.1.3. Types of loads and structural stresses

Dynamic power cables are subjected to various loads, including axial tension, bending, and torsional stresses. Understanding these loads and their impacts on the cable structure is crucial for ensuring its reliability and longevity. The structural integrity of the cable must be maintained under both static and dynamic conditions.

2.1.4. Factors affecting cable integrity and performance

Environmental factors such as temperature, salinity, and marine growth can affect the integrity of the cable. Proper material selection and protective measures are essential to mitigate these effects. For example, the use of anti-corrosion coatings and protective sheaths can help extend the operational life of the cable.

2.2. Dynamic cable system design

The COREWIND project represents a significant step forward in the renewable energy sector, particularly in the domain of offshore wind power. As offshore wind farms transition from fixed bottom structures to floating platforms, the need for robust and optimized dynamic cable systems becomes paramount. These cables are crucial for transmitting electricity generated by offshore wind turbines to the onshore grid, while being able to handle the demanding marine environment.

COREWIND is dedicated to the advanced optimization of dynamic cable design, focusing on enhancing the performance and reliability of floating offshore wind systems. By integrating cutting-edge technologies, sophisticated modeling, and comprehensive testing procedures, COREWIND aims to develop innovative solutions that address the mechanical, electrical, and environmental challenges faced by dynamic cables.

2.2.1. Dynamic cables review

The conventional configuration of a wind farm comprises a series of turbines, interconnected by cables, which collectively constitute a "string" of turbines. In larger wind farms, multiple strings may be present. The aforementioned strings then feed into an offshore substation (OSS). Cables that traverse the distance between turbines in a given string and ultimately reach the offshore substation are referred to as array cables (Fig. 5). The cables that extend from the offshore substation to the mainland are known as export cables. Subsequently, the power is transferred to an on-shore substation (SS) before its integration into the grid. In larger wind farms, backlink array cables may also be installed to facilitate the interconnection of two neighboring strings. In the event of an emergency where a fault within the farm results in the severing of a circuit in one string, the power from that string may be transmitted through the back-link cable and through the intact neighboring string. The power transmitted through this backlink is frequently constrained by the array cable design in the string that has been optimized for normal operation, driven by CAPEX reduction initiatives. To develop a cost-effective solution, the wind farm cable design must be customized for the specific project and site requirements due to the high number of possible variations.

Cross Section
Cables are classified according to their electrical voltage designation, which is typically expressed as U_0/U (Um) (Fig. 6):

- U_0 represents the rated root **mean square (RMS)** voltage between each conductor and the screen.
- U is the RMS voltage between two conductors, which can be approximated as U=1.73U_0.
- Um denotes the maximum RMS voltage between any two conductors.
- RMS refers to the root mean square value for an equivalent direct current (DC) voltage, which is equal to the peak voltage divided by the square root of two for a sine wave signal.

Ancillaty equipment Ancillary equipment for dynamic power cables in offshore wind farms and other marine applications includes various components that support the in-

Figure 6: Power cable cross section [15].

stallation, operation and maintenance of the cables. This equipment (Fig. 7) ensure the structural integrity, performance, and longevity of power cable systems.

- Buoyancy modules: Syntactic foam elements encapsulated in a polyethylene structure that are distributed along sections of the dynamic cable to provide floating assistance. They decouple the floating platform motions from the touchdown point, while at the same time reduce the hang-off loads on the cable clamp on the platform. They are typically installed in a 'lazy-wave' configuration.
- Bend stiffeners: Cone-shaped polyurethane elements, installed at the cable's end connections (e.g., at the device connector). They are used to add local transition stiffness to the cable in order to help mitigate the bending stress caused by the motions of the device.
- Bend restrictors: Polyurethane interlocking elements, typically installed at the interface between flexible and rigid structures, to prevent over-bending. They are designed to lock at a maximum curve radius when subject to a specified external load. The bend restrictor is usually the choice when (quasi-)static loads act on the cable, as opposed to bend stiffeners, which are more suited for damping dynamic loads.
- Cable protectors: Polyurethane half-shell sleeves that are installed at the cable touchdown point to provide both impact and abrasion resistance

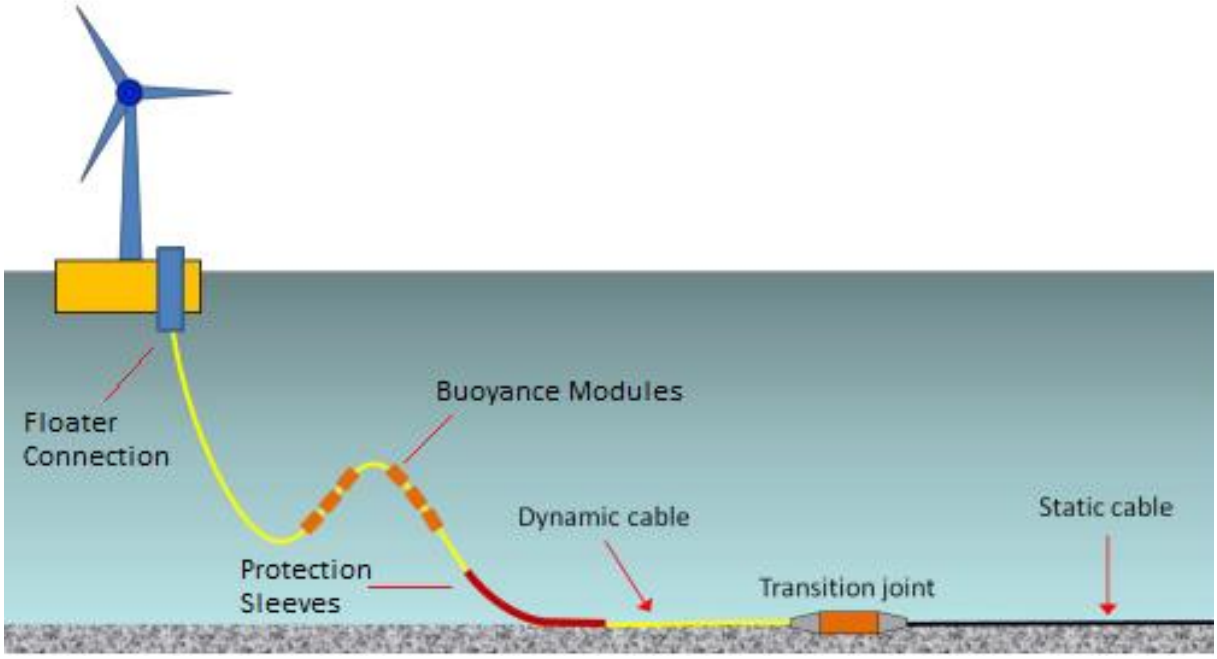

Figure 7: Dynamic power cable components [15].

2.2.2. Installation and maintenance techniques

Site Surveys

Site surveys are typically conducted prior to the engineering and installation phase to provide a project risk assessment. They provide information on the subsea terrain, topography, soil properties, and include hazard identification, hazard, and operability studies, and/or failure mode and effect analysis (FMEA) to outline the project-specific conditions. Generally, two types of surveys are performed:

Geophysical Survey: The geophysical survey is a non-penetrating survey. A vessel traverses the project site and emits pulses through a magnetometer. This approach can be used to identify nearby boulders, shallow faults and debris flows. Seismic testing is also conducted. By sending seismic pulses through powerful air guns, different layers of the seafloor can be identified down to a certain depth. Figure 5.1-1 shows an illustration of a geophysical survey. In addition to the survey vessel, a seafloor hydrophone is shown on the left side of Figure 5.1-1. It is used to detect seismic energy in the form of pressure changes underwater during the seismic survey.

Geotechnical Survey: Geotechnical surveys involve soil sampling and soil testing. Drilling can be used to collect 6m soil samples for laboratory analysis to determine soil properties. In addition, cone penetration tests are used to test the resistance of the seabed to the penetration of a test cone object.

Cable Vessels

In order to ensure a seamless installation of the dynamic cables following the hook-up, the selection of the installation vessel is of paramount importance. The choice of installation vessel depends on several factors, including cable design, cable length, depth of water, deployment area, prevailing environmental conditions, and the costs involved. It is important to note that the installation of cables in deeper waters presents a greater challenge than in near-shore operations. It is not feasible to use simple tugboats for the handling of grid connections via dynamic cables. Consequently, the deployment of larger and more specialized vessels is necessary [8]. The vessels used for dynamic cable installations are typically cable barges or cable laying ships. The latter type of vessel is typically more costly than cable barges because of its specialization in cable handling. The following factors should be taken into account when selecting cable installation vessels.

- Adequate storage for the cable lengths and weight in drums, coils, or turntables
- Maneuverability to determine the accuracy of the laid cable on the selected route
- Tension control equipment, tension measuring instrumentation, and Cable Deployment System
- Deck facilities for cable installation and recovery for repair
- Workshop facilities for equipment repair and cable jointing
- Control rooms for all equipment and data logging system
- Global positioning system for accurate positioning of the cable on the ocean floor
- Navigation and propulsion system to hold the vessel on station

Figure 8: Cable installation vessel [25].

Cable laying to WTG

The initial end of the cable must be pulled into the offshore unit. Subsequently, the pulling head / cable end is lifted overboard, aligned in front of the entry point of the offshore unit, and lowered toward the seabed in a controlled manner while the cable is paid out from

the cable vessel.

As a first step, the cable lay vessel will proceed to lay the cable on the seabed, after which the other end of the cable will be placed in close proximity to the J-tube of the next platform. Subsequently, a remotely operated vehicle may be utilized to establish a connection between the aforementioned free end of the cable and the pre-installed messenger wires, thereby facilitating the subsequent retrieval and connection of the cable.

The second end of the cable is then pulled into the offshore unit. Two methods are available for cable installation:

- Bight laydown: The cable end is laid on the seabed in the form of an S-shaped or W-shaped bight by navigating the installation vessel with great precision. Subsequently, the pulling head with the attached pulling line is lowered to the seabed, and the cable is pulled into the offshore unit.
- Deployment Quadrant: The cable is placed in a deployment quadrant, supported by a crane, winch system, or the A-frame of the vessel. As the quadrant is lowered towards the seabed, the cable is simultaneously pulled in.

2.2.3. Revision of cost evaluation

Different power cables are used in the Floating Offshore Wind Power Plant (FOWPP) such as dynamic and static inter-array cables as well as export cables. Different sections of the cable are used depending on the power to be transmitted. Thus, in general, the total cable cost includes the sum of each cable cost [5]:

$$C_{total} = \sum C_{pc} \cdot L_{pc} \cdot N_{pc} \tag{1}$$

Where CPC is the cost of a single cable in [€/m], L_{pc} the length in [m] and N_pc the number of this cable used. The cable cost used in (Eq.1)is per unit of length and is estimated as an exponential function, as follows:

$$C_pc = c1 + c3 \cdot \exp C3 \cdot S \tag{2}$$

According to [5], the cost of dynamic cables is more expensive than the equivalent static cables. Those are about $30-50\%$ more expensive for cables up to 33kV and range $60-90\%$ for cases up to 66kV.

2.2.4. Design practices

Guidance for dynamic cable system design is summarized in this section to facilitate the targeted development of floating wind farms, more information can be consulted on the

Dynamic Power Cable	Static Power Cable
Image source: JDR Cable Systems 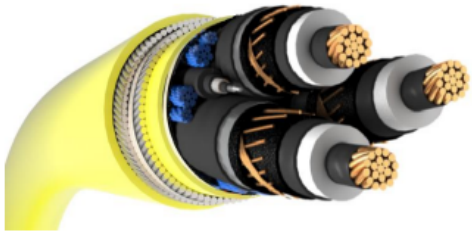	Image source: JDR Cable Systems 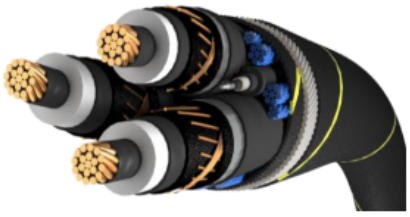
Outer Protective Sheath	Light Protective Rovings
Even number of Contra-helical Armour Wire Strength Member Layers	Single Armour Wire Strength Member Layer
Inner Bedding Layer Sheath	Inner Bedding Layer Rovings
Twisted Triad Bundle of Fibre Optic Cable and Electrical Cores with Wire based Screen	Twisted Triad Bundle of Fibre Optic Cable and Electrical Cores with Screen
Good Torsional Balance Greater Axial Strength (Max Tension) Greater Fatigue Resistance Greater Bend Stiffness Greater Weight and Outer Diameter Greater Abrasion Protection and Impact Resistance	Coil-able for low cost basket vessels Sufficient Axial Strength for shallow installation Light Weight Greater Flexibility (Smaller Minimum Bend Radius)

Figure 9: Comparison between static and dynamic cables [15].

Table 1: Cost of static cable [5].

Voltage (kV)		Cost Coefficient			Range	Units	Year	Ref.
Rated	Max	c1	c2	c3	(MVA)			
6.6	7.2	67.63	8.24	0.44	[2.9, 7.5]	k€/km	-	-
11	12	49.37	16.32	0.22	[4.8, 12.5]	k€/km	-	-
22	24	−1.27	50.66	0.07	[9.5, 27.2]	k€/km	-	-
33	36	−35.29	80.17	0.04	[17.0, 44.0]	k€/km	-	-
66	72.5	−57.35	105.20	0.02	[34.3, 94.3]	k€/km	-	-
132	145	−1337.00	1125.00	3.5×10^{-3}	[121.1, 188.6]	k€/km	-	-
MV	ns	0.5–2.0	0	0	ns	k£/m	2015	
22	ns	0.284×10^{6}	0.583×10^{6}	6.15×10^{-2}	[10, 45]	SEK/km	2003	
33	ns	0.411×10^{6}	0.596×10^{6}	4.1×10^{-2}	[15, 67.5]	SEK/km	2003	
66	ns	0.688×10^{6}	0.625×10^{6}	2.05×10^{-2}	[35, 135]	SEK/km	2003	
132	ns	1.971×10^{6}	0.209×10^{6}	1.66×10^{-2}	[100, 230]	SEK/km	2003	
220	ns	3.181×10^{6}	0.11×10^{6}	1.16×10^{-2}	[290, 385]	SEK/km	2003	
MV	ns	300–800	0	0	ns	€/m	ns	
HV	ns	1000–2000	0	0	ns	€/m	ns	
132	ns	7.471	39.28	1.40×10^{-2}	[150, 189] *	£/m	2008	
220	ns	−1044	963.4	1.91×10^{-3}	[250, 315] *	£/m	2008	
33	ns	100–200	0	0	ns	€/m	2012	
132	ns	200–600	0	0	ns	€/m	2012	

Corewind website [15].

- Identify and prioritise the main drivers for the cable system design philosophy and moored platform design philosophy

Table 2: Cost of dynamic cable [5].

Voltage (kV)		Cost Coefficient			Range	Units	Year	Ref.
Rated	Max	c1	c2	c3	(MVA)			
6.6	7.2	94.69	11.54	0.44	[2.9, 7.5]	k€/km	-	-
11	12	69.12	22.85	0.22	[4.8, 12.5]	k€/km	-	-
22	24	−1.78	70.92	0.07	[9.5, 27.2]	k€/km	-	-
33	36	−49.42	112.20	0.041	[17.0, 44.0]	k€/km	-	-
MV	ns	300–800	0	0	ns	€/m	2013	

- Undertake initial cable design prior to finalising mooring system design
- Set reasonable limits for moored platform offset distances relative to water depth
- Clearance limits from sea surface and seabed should be defined upfront and should be provided relative to environmental condition
- Dynamic cable emergency disconnection system should inform platform structure cable pathway and connection locations
- Marine growth at site should be reviewed to identify accurate profiles ahead of cable system development
- Cable connection point to the structure should be selected to minimise motion imparted into the cable, while allowing for installation
- Dynamic cable modelling should inform cabling J-tube structure exit design
- Hardware optimization studies specific for site and platform motion conditions are needed to reduce system costs
- Consider development of an optimized cabling system for floating wind typically will require longer upfront project analysis durations than O&G applications

2.3. Optimization methodology

Optimization methods involve using computational models to simulate different cable configurations and assess their performance. Techniques such as finite element analysis (FEA) and computational fluid dynamics (CFD) are commonly used. These methods allow for a detailed analysis of the DPC configuration.

Software tools such as OrcaFlex and ANSYS are used to model and analyze the behavior of dynamic power cables under various conditions. These tools help engineers optimize cable design for improved performance and reduced costs. By simulating real-world conditions, these tools enable the identification of potential issues and the development of effective solutions.

2.3.1. Optimization algorithm

Optimization in engineering involves using mathematical techniques to find the best possible solution to a problem within given constraints. This process is crucial in various engineering fields, such as mechanical, electrical, civil, and industrial engineering.

Complex systems can be improved by performing unconstrained optimizations. In which case, the best configuration is found by minimizing a function through an iterative process, where the accuracy of the solution depends on both the characteristics of the function being optimized and the algorithm applied.

The Steepest Descent Method, also known as the Gradient Descent Method, is an iterative optimization algorithm used to find the local minimum of a function. For an unconstrained optimization problem, the method proceeds as follows.

I. Initialization

- **Select an Initial Point:** Choose an initial guess $\mathbf{x}_0$ for the solution.

II. Compute the Gradient

- **Compute the Gradient:** At each iteration k, compute the gradient of the objective function $\nabla f(\mathbf{x}_k)$ at the current point $\mathbf{x}_k$. The gradient $\nabla f(\mathbf{x}_k)$ is a vector pointing in the direction of the steepest ascent of the function.

III. Determine the Step Size

- **Choose a Step Size (Learning Rate):** The step size α_k determines how far you move in the direction of the negative gradient. It can be a fixed value or determined adaptively. Common techniques for adaptive step size include backtracking line search or exact line search.

IV. Update the Solution

- **Update the Solution:** Compute the next point $\mathbf{x}_{k+1}$ using the formula:

$$\mathbf{x}_{k+1} = \mathbf{x}_k - \alpha_k \nabla f(\mathbf{x}_k)$$

  where α_k is the step size and $\nabla f(\mathbf{x}_k)$ is the gradient of the function at $\mathbf{x}_k$.

V. Check for Convergence

- **Convergence Check:** Determine if the algorithm has converged. This can be done by:
  - Checking if the norm of the gradient $\|\nabla f(\mathbf{x}_k)\|$ is below a specified tolerance.

  - Checking if the change in function value $f(\mathbf{x}_{k+1}) - f(\mathbf{x}_k)$ is smaller than a given tolerance.
  - Checking if the change in the solution $\|\mathbf{x}_{k+1} - \mathbf{x}_k\|$ is below a specified tolerance.

VI. Iterate

- **Repeat Steps II-IV:** Continue the process until convergence is achieved.

3. METHODOLOGY

This section describes a systematic approach used in the investigation to optimize the configurations of lazy wave riser systems. This study integrates both theoretical and practical frameworks to address the complexities involved in the design and implementation of a DPC in a WTG. The methodology is divided into several key components: the selection of the base case scenario , the cable properties, and the consideration of environmental conditions. Furthermore, this section delves into the load case definitions, static and extreme analyzes, and the optimization process, including variable selection and parameter measurement. The final subsections focus on fatigue analysis, highlighting stress factors and the S-N curves necessary to estimate damage.

3.1. Base case (IEA Wind TCP Task 37)

The VolturnUS-S (Fig. 10) is a semi-submersible platform developed by the IEA as a benchmark study, its properties are described in (Tab. 3). OrcaFlex provides the case setup for the tower, platform, mooring system, and water depth.

As the tension conveyed from the DPC to the platform is relatively smaller compared to the tensions from the mooring lines, the excursion is determined without the cable, and later that excursion is the input for the dynamic analysis of the DPC.

Table 3: VolturnUS-S semi-submersible platform properties [1].

Parameter	Units	Value
Hull Displacement	m^3	20,206
Hull Steel Mass	t	3,914
Tower Interface Mass	t	100
Ballast Mass (Fixed/Fluid)	t	2,540/11,300
Draft	m	20
Freeboard	m	15
Vertical Center of Gravity from SWL	m	-14.94
Vertical Center of Buoyancy from SWL	m	-13.63
Roll Inertia about the Center of Gravity	kg-m^2	1.251E+10
Pitch Inertia about Center of Gravity	kg-m^2	1.251E+10
Yaw Inertia about Center of Gravity	kg-m^2	2.367E+10

3.2. Dynamic power cable

Among the technological developments that facilitate the reduction of LCOE, several independent studies have shown that the use of cable arrays operating at 66 $[kV]$ instead

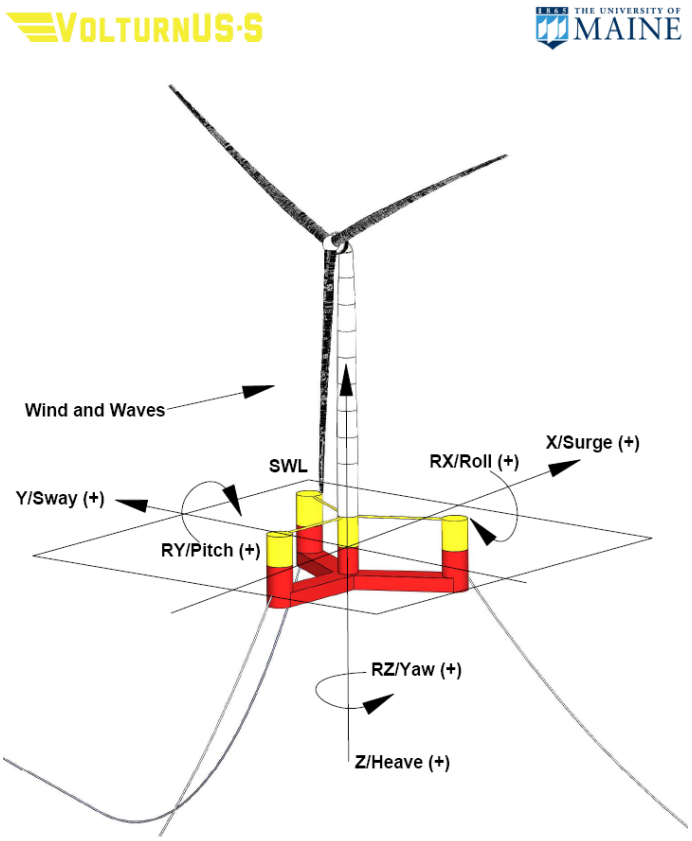

Figure 10: VolturnUS-S reference platform 15MW turbine[1].

of 33 $[kV]$ presents considerable advantages in the context of typical offshore wind farm systems. The primary cost reduction drivers for employing 66 $[kV]$ instead of 33 $[kV]$ while maintaining the same total output power are as follows.

- The use of 66 $[kV]$ array cables instead of 33 $[kV]$ cables allows the transportation of twice the power over a single cable, reducing the size of the cable and the investment in these cables and their installation.
- The number of cables entering the offshore substation is reduced, resulting in a reduction in the number of J-tubes.
- The use of larger turbines with reduced unit power allows for a reduction in the number of turbines and associated array cables.
- The number of transformers, and switches, as well as the space required for these items are reduced.

The cable design should ensure secure transmission of the energy produced by the 15 [MW] WTG. Cables are classified according to a particular voltage and, depending on the power transferred, the dimensions of the cable may vary to handle the current. As a preliminary estimation, excluding losses, the design current can be approximated by Ohm's law:

$$P = I \cdot V \tag{3}$$

When selecting the diameter of the cable, it is necessary to keep in mind that normally the bigger the cable, the more current can pass through it. According to Ohm's law (Eq. 3) $I = P/V$ for a rated power of ($\mathbf{P} = 15$ [MW]), a ($\mathbf{V} = 66$ [kV]) cable should be able to transfer at least $\mathbf{I} = 227$ [A]. From the manufacturer catalogs, it is necessary to select a cable that satisfies such requirement

Muk et al. [3] conducted an analysis on the fatigue of inter-range (66 [kV]) power cables, the cable properties are described in (Tab. 4). The properties provide a useful reference for initial design, but in more advanced design stages, this information should be updated with data supplied by manufacturers.

Table 4: Power cable properties [3].

Parameter	**Dimension**	**Value**
Voltage rating	kV	66
Outer diameter	m	0.116
Mass per unit length	kg/m	25.0
Torsional stiffness	kNm^2/deg	38.0
Axial stiffness	MN	362
Bend stiffness	kNm^2	6.74
Tension at conductor yield	kN	885
Minimum bending radius	m	1.8
Maximum curvature	1/m	0.556
Drag coefficient	$\sim$	1.2
Added mass coefficient	$\sim$	1.0

3.2.1. Lazy weave configuration

The lazy wave (Fig. 11) is among the most widely used configurations for dynamic cables. The system is intended for easy configuration and can accommodate marine growth at levels appropriate for its depth. In shallow waters, higher levels of marine growth might be managed by adding buoyancy modules during the system's operational life. The system has been used effectively in deep-water applications.[15]

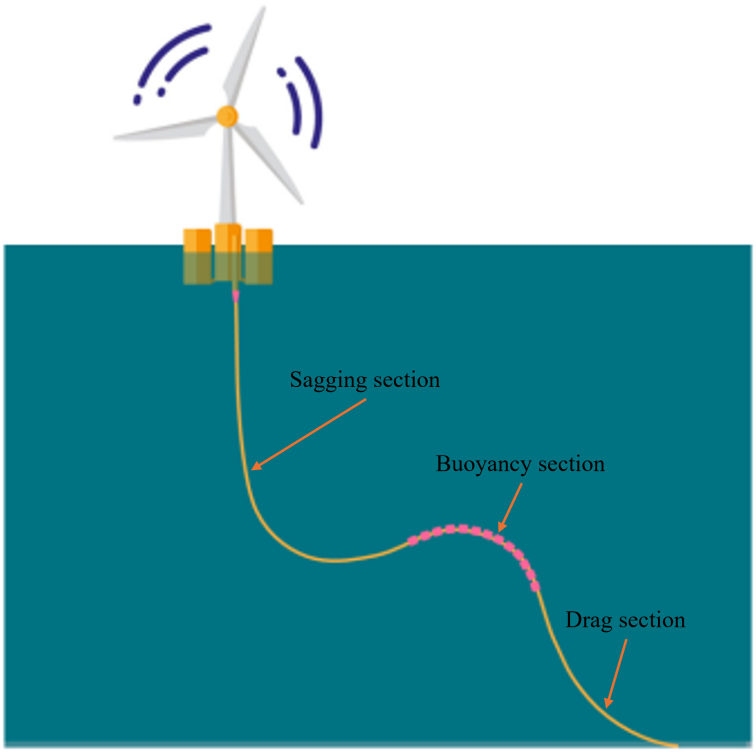

Figure 11: Lazy wave configuration [15].

The main purpose of the buoyancy section (floaters) is to decouple movement between the platform and the **touch down point (TDP)**; however, excessive buoyancy leads to increased cable curvature across the sagging and buoyancy segments. On the other hand, a larger sagging section results in increased tension at the **hang-off point (HOP)**.

3.3. Environmental conditions

Environmental loads are forces exerted on structures, such as offshore platforms, bridges, or buildings, due to natural environmental conditions. In the context of offshore engineering, environmental loads are particularly crucial because they significantly impact the design, stability, and operational safety of structures such as subsea cables, floating wind turbines, and oil rigs.

3.3.1. Loads from wind

Wind loads are one of the primary environmental forces that must be considered in the design and analysis of offshore **floating wind turbines (FWT)**. These loads result from the pressure exerted by the wind on the exposed surfaces of a structure.

Wind loads are dynamic and vary in intensity depending on factors such as wind speed, direction, and turbulence. For offshore structures, wind loads are particularly critical due

to the open-sea environment, where wind speeds can be significantly higher and more sustained than on land. The loads are typically described by the wind pressure acting on a structure, which is a function of the wind speed squared.

Mathematical modeling of wind loads

The basic formula to calculate the wind load on a surface is as follows:

$$F_w = \frac{1}{2} \cdot \rho \cdot C_d \cdot A \cdot V^2 \tag{4}$$

Where:

- F_w is the wind load force.
- ρ is the air density.
- C_d is the drag coefficient.
- A is the projected area of the structure facing the wind.
- V is the wind speed.

3.3.2. Loads from waves

Wave loads are one of the most significant environmental forces acting on offshore structures. These loads result from the interaction between ocean waves and the structure, leading to dynamic forces that can significantly influence the design, stability, and operational safety of offshore installations such as platforms, wind turbines, and subsea cables.

Ocean waves are generated primarily by wind and their characteristics are influenced by factors such as wind speed, duration, and the distance over which the wind blows. The forces exerted by waves on a structure are complex and depend on the height, period, and direction of the wave, as well as the shape, size, and orientation of the structure.

Wave loads can be broadly classified into two types:

- **Inertia Forces**: These are associated with the acceleration of the water particles within a wave and typically dominate in deep water, where the wave height is large relative to the wavelength.
- **Drag Forces**: These are related to the relative velocity between the water particles and the structure. Drag forces are more significant in shallow water, where waves tend to be steeper.

Mathematical modeling of wave loads

The analysis of wave loads typically begins with the characterization of wave behavior using wave theories. Depending on the water depth and wave conditions, different wave theories may be applied, including linear (Airy) wave theory, Stokes theory, and nonlinear theories.

For practical design, wave loads on offshore structures are often calculated using the Morison's equation, which accounts for both inertia and drag forces. Morison's equation for the wave force per unit length on a cylindrical member is given by:

$$F(t) = \frac{1}{2}\rho C_D D|u(t)|u(t) + \rho C_M \frac{\pi D^2}{4}\frac{du(t)}{dt} \tag{5}$$

Where:

- $F(t)$ is the total wave force per unit length at time t.
- ρ is the density of water.
- C_D is the drag coefficient.
- C_M is the inertia coefficient (added mass).
- D is the diameter of the cylindrical member.
- $u(t)$ is the velocity of the water particles induced by wave at time t.
- $\frac{du(t)}{dt}$ is the acceleration of the water particles induced by wave at time t.

Statistical represetation of waves

The Joint North Sea Wave Project (JONSWAP) spectrum is a widely used wave spectrum that provides a more accurate representation of wave conditions in fetch-limited seas, such as the North Sea. The JONSWAP spectrum extends the Pierson-Moskowitz spectrum by introducing a peak enhancement factor, making it better suited for younger, developing wave fields.

The JONSWAP spectrum [26] is expressed as:

$$S_j(\omega) = \frac{\alpha g^2}{\omega^5}\exp\left[-\frac{5}{4}\left(\frac{\omega_p}{\omega}\right)^4\right]\gamma^r \tag{6}$$

$$\alpha = 0.076\left(\frac{U_{10}^2}{F\ g}\right)^{0.22}$$

$$\omega_p = 22\left(\frac{g^2}{U_{10}F}\right)^{1/3}$$

Where:

- U_{10} is the average wind speed meassured at 10 meters above the sea surface.
- $S(\omega)$ is the wave energy spectral density at frequency ω.
- g is the acceleration due to gravity.
- ω_p is the peak frequency, corresponding to the highest energy content in the spectrum.
- γ is the peak enhancement factor, typically ranging between 1 and 7, with a standard value of 3.3 for the North Sea.
- σ is the spectral width parameter, where $\sigma = 0.07$ for $f \leq f_p$ and $\sigma = 0.09$ for $f > f_p$.
- α is the Phillips constant, related to the wave height.
- F is the distance from a lee shore, called the fetch, or the distance over which the wind blows with constant velocity.

3.3.3. Loads from current

Underwater current forces are significant environmental loads that impact offshore structures, including wind turbine generators, platforms, and subsea installations. These forces arise from the movement of water masses and can vary greatly depending on factors such as current speed, direction, and depth. Accurate estimation and management of these forces are crucial to ensuring the stability and integrity of offshore structures.

Underwater currents are the result of various natural phenomena, including tidal movements, wind-driven waves, and oceanic circulation patterns. These currents can be categorized as follows.

- **Tidal Currents**: Result from the gravitational pull of the moon and sun, creating predictable variations in water flow, including both flood and tide receding currents (ebb).
- **Residual Currents**: Generated by the interaction of tidal currents with the seabed and other structures, leading to complex, non-uniform flow patterns.
- **Geostrophic Currents**: Driven by large-scale pressure gradients and the Coriolis effect, these currents can be significant in deep ocean regions.
- **Local Currents**: Resulting from wind and wave interactions, often varying in strength and direction with changing weather conditions.

Calculation of current forces

The forces exerted by underwater currents on a structure can be calculated using principles similar to those used for wind loads. The key factors include:

- **Current Speed (V)**: The velocity of the water flow, which directly influences the magnitude of the force.
- **Drag Coefficient (C_d)**: A dimensionless factor representing the resistance of the structure to the current. This coefficient depends on the shape, surface roughness, and orientation of the structure.
- **Projected Area (A)**: The area of the structure that is exposed to the current flow.

The basic formula to estimate the force due to underwater currents is the following.

$$F_c = \frac{1}{2} \cdot \rho \cdot C_d \cdot A \cdot V^2 \tag{7}$$

Where:

- F_c is the current force.
- ρ is the density of seawater, typically around 1025 kg/m^3.
- C_d is the drag coefficient, which varies based on the geometry and orientation of the structure.
- A is the projected area of the structure facing the current.
- V is the current speed.

3.3.4. Short term sea state

To define a sea state, the significant wave height, peak period, mean wind speed, and current speed (Hs, Tp, Uw, Uc) must be specified. DNV-RP-C205 [9] provides some information on the wave conditions for different nautic zones (Fig. 12) around the world.

In this study the zone 16 is considered (see Fig. 12), some data is obtained form *Puertos del estado* [24]. This is a Spanish institution that gives free access to oceanographic data, from there the scatter diagram and the Weibull distribution function of the wind speed (Figs. 13, 14) can easily be obtained. The buoy *Villano Sisargas* is selected because the depth of water in this zone is around 200 [m] and this matches the water depth for the platform introduced in the base case.

The *Villano-Sisargas* buoy is located off the Galician coast, near Cape Vilán. This buoy is part of the Puertos del Estado observation network and is used to monitor sea conditions, including wind, waves, and other meteorological and oceanographic parameters.
Some key data from the buoy are:

- Longitude: -9.210 E
- Latitude: 43,500 N

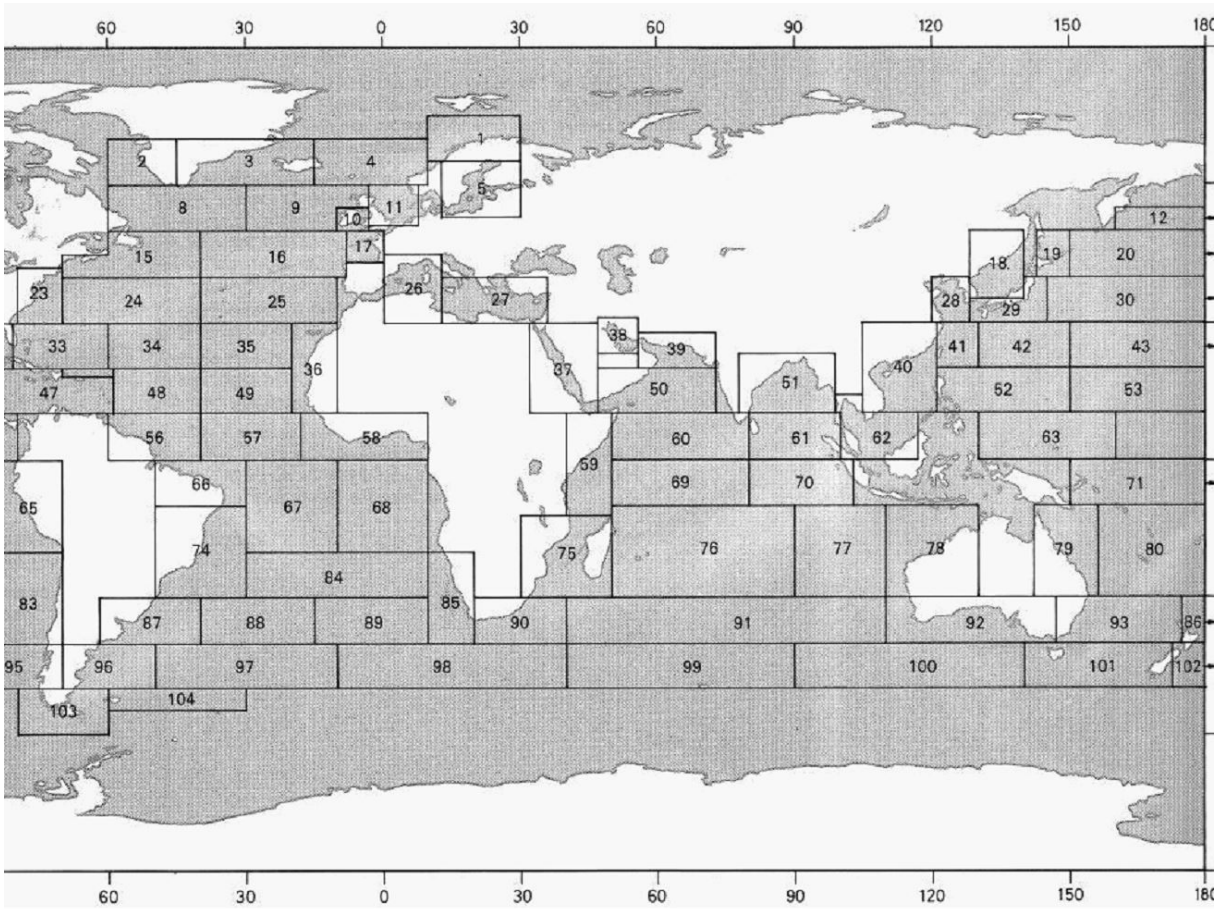

Figure 12: Nautical zones worldwide [9].

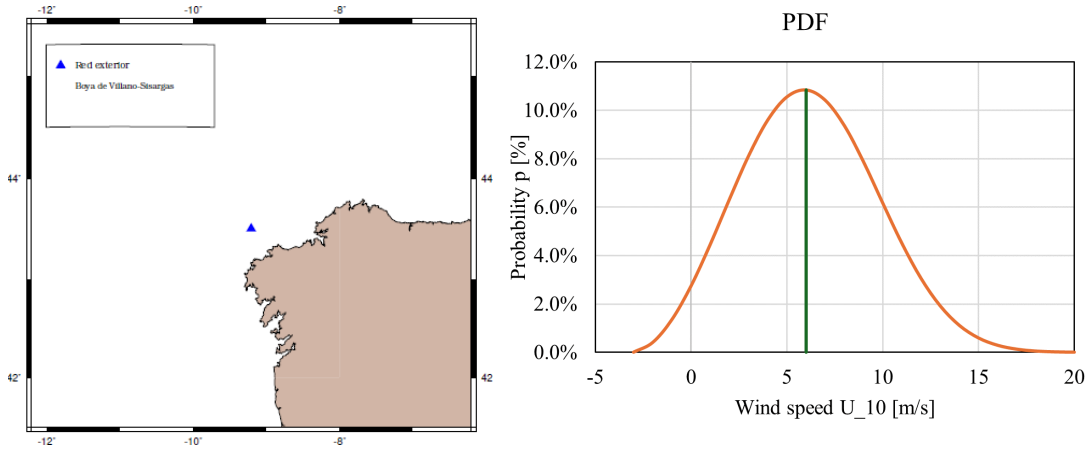

(a) Villano Sisargas Buoy location. **(b)** PDF for the mean wind speed.

Figure 13: Mean annual wind speed regimen (Mode velocity 6$[m/s]$) [24].

- Depth: 386,000 m

In this location, the mode speed is 6 [m/s] with a probability of 10.08%. Later, to estimate the short-term sea state, a new mode speed needs to be determined for each wave condition presented in the scatter diagram (Fig. 14).

The annual mean wind speed is described with a Weibull distribution (Eq. 9). Where α is the shape parameter (normally between 0.5 and 3.5), β is the scale parameter (it must be greater than zero), and finally γ is the location parameter (it must be greater than all registered values). The values provided for this location are: $\alpha_U = 2.88$, $\beta_U = 10.46$, $\gamma_U = -3.12$.

The scatter diagram (Fig. 14) shows the probability of a pair Ts, Hs to happen. The significant wave height (H_s) and peak period (T_p) cover the range of probable sea states. A higher probability means that wave condition is more likely to occur.

Hs\Tp	2	3.0	4.5	6.0	7.5	9.0	10.5	12.0	13.5	15.0	16.5	0
0.5	0.0%	0.0%	0.0%	0.0%	0.0%	0.0%	0.0%	0.0%	0.0%	0.0%	0.0%	0.0%
1.0	0.0%	0.0%	0.2%	0.8%	1.6%	1.4%	0.7%	0.2%	0.1%	0.0%	0.0%	5.0%
1.5	0.0%	0.0%	0.3%	1.8%	3.3%	4.4%	3.8%	1.2%	0.3%	0.1%	0.0%	15.2%
2.0	0.0%	0.0%	0.1%	2.3%	2.7%	4.1%	6.0%	3.1%	0.8%	0.2%	0.1%	19.4%
2.5	0.0%	0.0%	0.0%	1.3%	2.9%	2.4%	4.7%	3.7%	1.1%	0.3%	0.1%	16.5%
3.0	0.0%	0.0%	0.0%	0.2%	2.1%	1.6%	3.2%	3.8%	1.4%	0.3%	0.2%	12.8%
3.5	0.0%	0.0%	0.0%	0.0%	0.8%	1.2%	2.1%	3.1%	1.5%	0.3%	0.1%	9.2%
4.0	0.0%	0.0%	0.0%	0.0%	0.2%	0.8%	1.3%	2.4%	1.7%	0.4%	0.2%	7.0%
4.5	0.0%	0.0%	0.0%	0.0%	0.0%	0.4%	0.8%	1.7%	1.5%	0.4%	0.2%	5.1%
5.0	0.0%	0.0%	0.0%	0.0%	0.0%	0.2%	0.5%	1.0%	1.3%	0.4%	0.1%	3.4%
5.5	0.0%	0.0%	0.0%	0.0%	0.0%	0.1%	0.5%	1.3%	2.4%	1.5%	0.7%	6.5%
0	0.0%	0.0%	0.6%	6.5%	13.7%	16.4%	23.6%	21.5%	11.9%	4.0%	1.8%	100.0%

Figure 14: Scatter diagram for buoy Villano Sisargas [24].

As mentioned in [19], the raw data indicate that the dependency of the distribution parameters for T_p on U_w is limited. Then a simplified method is proposed in which the distribution parameters for T_p are only dependent on H_s, which simplifies the joint **probability density function (PDF)** of U_w, H_s, and T_p. To create the short-term sea state, 20 points are selected from the scatter diagram (Fig. 14). Then the method proposed (Eq. 8) is used to estimate the mode speed.

The joint probability $f_{U,Hs,Tp}(u,h,t)$ is approximated as the product of the PDF for the wind speed $f_U(u)$, times the joint PDF for wave height given a wind speed $f_{Hs|U}(h|u)$, times the joint PDF for the peak period given the wave elevation $f_{Tp|Hs}(t|h)$.

$$f_{U,Hs,Tp}(u,h,t) \approx f_U(u) \cdot f_{Hs|U}(h|u) \cdot f_{Tp|Hs}(t|h) \tag{8}$$

$$f_U(u) = \frac{\alpha_u}{\beta_u}\left(\frac{u-\gamma_u}{\beta_u}\right)^{\alpha_u - 1} \exp\left(-\left[\frac{u-\gamma_u}{\beta_u}\right]^{\alpha_u}\right) \tag{9}$$

The PDF of the wind speed corresponds to the mean annual wind speed measured at 10

[m] above the sea surface, every 10 minutes. The parameters of the Weibull distribution α_u, β_u, and γ_u are provided in [24].

$$f_{Hs,U}(h|u) = \frac{\alpha_{uh}}{\beta_{uh}} \left(\frac{h}{\beta_{uh}} \right)^{\alpha_{uh}-1} \exp\left(- \left[\frac{h}{\beta_{uh}} \right]^{\alpha_{uh}} \right) \tag{10}$$

The conditional probability of Hs given u is given by (Eq.10), where α_{uh} and β_{uh} are the parameters of the Weibull distribution, given by the following relation:

$$\alpha_{uh} = a1 + a2 \cdot u^{a3} \tag{11}$$

$$\beta_{uh} = b1 + b2 \cdot u^{b3} \tag{12}$$

The same applies for the condition probability Tp given Hs, this PDF is represented by an exponential function (Eq. 13). Where t is the wave period and h is the significant wave height, and the variables μ_{th} and σ_{th} are given by the following relation:

$$f_{Tp,Hs}(t|h) = \frac{1}{t\sigma_{th}\sqrt{2\pi}} \exp\left(-\frac{1}{2} \left[\frac{\ln(t) - \mu_{th}}{\sigma_{th}} \right]^2 \right) \tag{13}$$

$$\mu_{th} = c1 + c2 \cdot h^{c3} \tag{14}$$

$$\sigma_{th} = d1 + d2 \cdot \exp\left(d3 \cdot h\right) \tag{15}$$

To obtain the mode velocity, the non-linear system is solved for each pair of H_s and T_P by maximizing the PDF of the joint probability equation (Eq. 8) and using the constants given in [19].

The **short-term sea states (STSS)** represent a collection of the most likely wave conditions; these are characterized by Hs, Tp, Uw, Uc, and their joint probability of occurrence, as illustrated in Tab. 5.

Table 5: Short term sea states.

Name	Period (s)	Height (m)	Wind Speed (m/s)	Current speed[m/s]	p (%)
STSS1	10.5	2	5.65	0.17	9.30%
STSS2	10.5	2.5	6.32	0.19	7.30%
STSS3	9	1.5	4.97	0.15	6.80%
STSS4	9	2	5.65	0.17	6.30%
STSS5	12	3	7.02	0.21	5.90%
STSS6	10.5	1.5	4.97	0.15	5.90%
STSS7	12	2.5	6.32	0.19	5.80%
STSS8	7.5	1.5	4.97	0.15	5.10%
STSS9	10.5	3	7.02	0.21	4.90%
STSS10	12	3.5	7.75	0.23	4.90%
STSS11	12	2	5.65	0.17	4.80%
STSS12	7.5	2.5	6.32	0.19	4.50%
STSS13	7.5	2	5.65	0.17	4.30%
STSS14	12	4	8.50	0.26	3.70%
STSS15	9	2.5	6.32	0.19	3.70%
STSS16	13.5	5.5	10.86	0.33	3.70%
STSS17	6	2	5.65	0.17	3.60%
STSS18	7.5	3	7.02	0.21	3.30%
STSS19	10.5	3.5	7.75	0.23	3.30%
STSS20	6	1.5	4.97	0.15	2.80%

3.4. Load case definition

3.4.1. Static analysis

The STSS 16 represents the toughest environmental conditions for wind speed, wave height, wave period, and current. Although its probability of occurrence is 3.7%, it is one of the STSS scenarios expected during regular operations.

In the static analysis of the cable, the platform is positioned at the reference system's center. The DPC is fixed to the platform and anchored on the seabed. The forces considered are the distribution of weight and buoyancy along the cable, and the current speed from the STSS 16.

3.4.2. Maximum offset estimation

The response to an extreme event (50 years) is also analyzed; Lin et al.[19] estimate such events for five European locations (Fig. 15). From these locations , **Site 3** is located inside the nautical zone 16 (Fig. 12), where the buoy *Villano Sisargas* is also located. The extreme condition evaluates the system's response to an extreme event that occurs once every 50 years. The load cases for this event are given in (Tab. 6).

Figure 15: European Offshore Sites [19].

Table 6: Extreme conditions [19].

Condition	Site 1	Site 3	Site 5	Site 14	Site 15
Condition with maximum Uw					
Uw (m/s)	23.7	28.3	27.5	33.6	27.2
Hs (m)	8.0	8.8	11.4	13.4	8.1
Tp (s)	12.2	11.9	13.5	13.1	10.0
Condition with maximum Hs					
Uw (m/s)	21.4	24.3	25.1	31.2	25.3
Hs (m)	10.2	12.1	14.0	15.6	9.5
Tp (s)	13.8	13.8	15.11	14.5	12.3

To estimate the maximum offset, various load directions are analyzed (Fig. 16). The WTG demonstrates its maximum horizontal mooring stiffness when the load case aligns with a

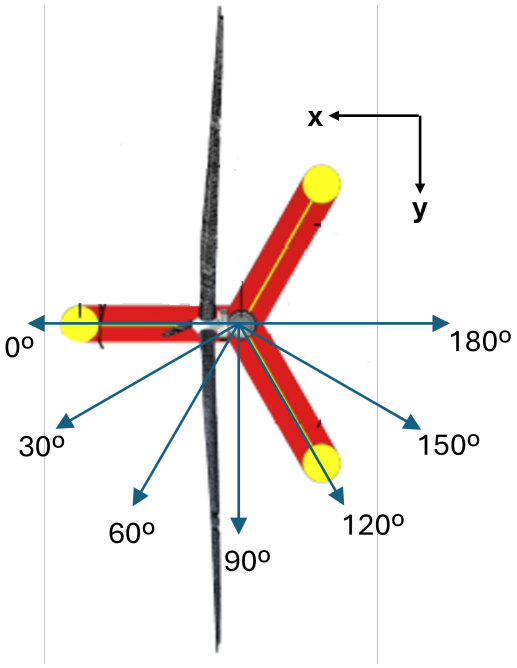

Figure 16: Wind/Wave/Current for maximum excursion estimation.

mooring line, such as at 60º and 180º. In contrast, the system shows reduced strength in directions 0º and 120º as reported in (Tab. 7).

The greatest displacement occurs when the aligned Wind/Wave/Current load acts in the 0º direction (Tab. 7). The offshore platform mooring systems exhibit the lowest horizontal stiffness in this direction, thus permitting the largest displacement of the platform. **This direction is used for all subsequent analyzes because it allows the maximum excursion (ΔL).**

Table 7: Maximum excursion for 50-year.

Direction	maxX	maxY	maxZ	ΔL [m]
0º	37.98	0.09	-0.66	**37.98**
30º	31.63	8.92	-0.63	32.87
60º	12.39	21.29	-0.58	24.64
90º	-8.12	31.63	-0.62	32.66
120º	-19.00	32.62	-0.66	**37.75**
150º	-23.57	22.79	-0.63	32.79
180º	-24.75	-0.21	-0.58	24.76

3.4.3. Extreme analysis

The load cases used in this section correspond to the 50-year return period condition found at **Site 3** (Tab. 6), and the load direction considered for the dynamic analysis is

the one that produces the largest offset (Tab. 7). Usually a storm lasts 3 hours, and when performing the dynamic simulation an additional time of 7 minutes is included at the beginning of the simulation to ignore the system startup data.

3.5. Optimization

The performance of the cable during its static equilibrium is measured in terms of tension at the HOP, minimum curvature in the sagging section, maximum curvature in the buoyancy section, and total length of the cable. The optimization is treated as a simple **unconstrained problem** P_{UNC} (Eq. 16), the step descent algorithm is implemented to minimize a function that evaluates the performance of the umbilical cable.

$$P_{UNC} = \begin{cases} Minimize f(x) \\ X \epsilon R^n \end{cases} \tag{16}$$

3.5.1. Weight function - f(x)

The objective function (Eq. 17), is an non dimensional function created to evaluate cable performance, based on the ratio of effective tension and curvature with respect to the recommended operational limits given by the manufacturer (f_i) and weight factors (c_i) set by the user.

$$f(x) = \sum_{i=1}^{n} \left[c_i \cdot fi \right], Where \sum_{i=1}^{n} c_i = 1 \tag{17}$$

An algorithm written in Python minimizes the problem by running a static analysis in OrcaFlex for each iteration. The optimal solution is difficult to find; that is why in the preset problem the algorithm stops after reaching a percentage of improvement in the system or when reaching a certain number of iterations (see App. B). Later, the new configuration is tested to estimate the fatigue life.

The system is complex and depends on many variables. The design variables considered in this study are the length of each section and the anchor position. (The buoyancy modules are implicitly included in the buoyancy section length).

3.5.2. Variables - X

As mention above the variables are:

- Sagging section
- Buoyancy section
- Drag section
- Anchor point

3.5.3. Measured parameters - fi

The functions f_i are non-dimensional functions that assess the relationship between the actual tension and curvature with the cable operational limits recommended by the manufacturers.

- f1 = T_{HOP}/T_{max} Evaluates the tension at the hang off point.
- f2 = f2 Evaluate the minimum required curvature in the sagging section, to decouple the cable motion.
- f3 = k/k_{max} Evaluates the maximum curvature in the buoyancy and drag section.
- f4 = $L_{cable}/Lmax$ Evaluates the total length of the cable.

$$f2 = \begin{cases} -k/k_{max} + 2k_{min}/k_{max}, & \text{if } k < k_{min} \\ k/k_{max}, & \text{if } k > k_{min} \end{cases} \tag{18}$$

The manufacturers recommend operation limits for the tension at the hang-off point and the minimum bending radius in the cable. The **minimum bending radius (MBR)** can be translated as the maximum curvature using the following relationship: $k_{max} = 1/MBR_{min}$.

Ideally, the minimum tension and curvature is achieved when the cable connecting the platform with the anchor point is a straight line. To avoid this from happening, it is important to consider a minimum curvature different than zero in the sagging section (Eq. 18); if not, the optimization algorithm will give a simple line.

The curvature developed in the buoyancy section depends on the separation of the floaters; if most of the floaters are concentrated in one zone (small spacing), the curvature is higher than distributing them all along the length of the buoyancy section. As the length of the sagging segment increases, the tension at the HOP increases, while the curvature decreases.

3.6. Fatigue analysis

The DPC is designed with fatigue considerations, where the resulting stress is a combination of tension and curvature. Choosing the correct configuration is crucial to ensure that the system achieves its intended **operational life of 32 years** (2y for installation and 30y for operation).

The dynamic simulation is divided into two stages; the first stage is necessary in order to avoid transient effects due to the start of the simulation and is set to 7min (420s), then the rest of the simulation lasts for 30 min (1800 s) as recommended in [4]. The total simulation will be 37min (2220s) for each STSS (Tab. 5).

Later in fatigue analysis, all simulations are accounted for a total time of one year by distributing the hours in all load conditions. Each STSS probability is multiplied by the number of hours in the year, to make an estimation of how many hours during a year that sea state might happen.

From solid mechanics, the total stress for a beam that undergoes elastic deformation can be approximated as the sum of stress produced by the effective tension and the stress produced to form a curvature in the cable. OrcaFlex [20] recommends using the factor stress method (Eq.19) to assess the stress produced in the cable, after evaluating different directions (θ), the highest value is considered representative for each location (s).

$$S = K_t T + K_c(C_x \sin\theta - C_y \cos\theta) \tag{19}$$

Where:

- **S** is the total stress in the cable.
- K_t**,** K_c are the tension and curvature stress factors, respectively.
- **T** is either wall tension or effective tension, as specified by the tension variable.
- θ is the circumferential location of the fatigue point.

3.6.1. Stress factors

The stress factor are constants that depend on the mechanical properties of the cable components. The curvature stress factor K_c provides the stress due to curvature when multiplied by the curvature. Similarly, the tension stress factor K_t when multiplied by the effective tension results in stress originating from tension.

The analytical approximations were introduced by [4]&[3]. Its mathematical deduction considering only two components (conductor c and armor a), the variables T (effective

tension) and K (curvature) can be obtained from quasi-static or FEM models and change along the cable's length. When multiplied by their respective stress factors (Eqs. 20-23), yield the stress generated within the cable (Eq. 19).

The stress factors for a cable made of two components can be approximated using the following equations:

$$\sigma_a = \left(\frac{1}{A_a + A_c \cdot E_c/E_a}\right) \cdot T + E_a \cdot \frac{d_a}{2} \cdot K$$

$$\sigma_c = \left(\frac{1}{A_c + A_a \cdot E_a/E_c}\right) \cdot T + E_c \cdot \frac{d_c}{2} \cdot K$$

$$K_t a = \frac{1}{A_a + A_c \cdot E_c/E_a} \tag{20}$$

$$K_t c = \frac{1}{A_c + A_a \cdot E_a/E_c} \tag{21}$$

$$K_c a = E_a \cdot d_a/2 \tag{22}$$

$$K_c c = E_c \cdot d_c/2 \tag{23}$$

Where:

- σ_a, σ_c are the total stresses, for the armour and the conductor, respectively.
- A_a, A_c are the sectional areas, for the armour and the conductor, respectively.
- E_a, E_c are the young modulus of the components.
- d_a, d_c are the diameters of the cable wire components.

Wire Properties

In order to determine the stress factors (K_t and K_c), certain mechanical properties (Tab. 8, 9) are necessary, and these values are usually supplied by manufacturers. In this thesis the values are taken from [3], note that this is an approximation and is recommended to be confirmed with Industry.

3.6.2. S-N curves

SN curves, or S-N curves (Stress-Number of cycles curves), are graphical representations used in material science to describe the relationship between the cyclic stress applied to a material and the number of cycles it can withstand before failure. These curves are crucial for understanding the fatigue life of materials. For cables, the S-N curves help predict how

Table 8: Wires geometrical properties [3].

Parameter	Dimension	Value
Number of steel wires	∼	138
Number of copper wires	∼	3
Diameter of steel	mm	4.28
Diameter of copper	mm	12.79
A steel	mm2	14.39
A copper	mm2	128.48

Table 9: Wires stress factors [3].

Parameter	Dimension	Value
A armour	m2	1.99E-03
A copper	m2	3.85E-04
E armour	kPa	2.00E+08
E copper	kPa	9.50E+07
d armour	m	4.28E-03
d copper	m	12.78E-03
kt armour	kPa/kN	461.06
kc armour	kPa/(rad/m)	4.28E+05
kt copper	kPa/kN	219.00
kc copper	kPa/(rad/m)	6.08E+05

long a cable can last under repeated loading and unloading cycles. The curve typically shows a decreasing trend, indicating that as the stress level increases, the number of cycles to failure decreases.

Conductor

Due to the non-linear stress-strain behavior of conductor, a traditional S-N curve for copper conductors in a dynamic power cable has limited application. Therefore, it is recommended to present the fatigue curves of copper as $\epsilon - N$ curves (Fig. 17) [17].

Armour

DNV recommended practices for fatigue design of offshore steel structures (DNV-RP-C203) in its Appendix D, gives the S-N (Fig. 18) curve for a high strength steel armour components subjected to mean tensile stresses. This curve is defined by the slope (m) and the intersection with the y-axis ($log(a)$) in a log-log scale. The recommended values are $m = 4.7$ and $log(a) = 7.446$ for components under seawater.

$$\Delta\sigma = a \cdot N^m \tag{24}$$

$$log(N) = log(a) - m \cdot log(\Delta\sigma) \tag{25}$$

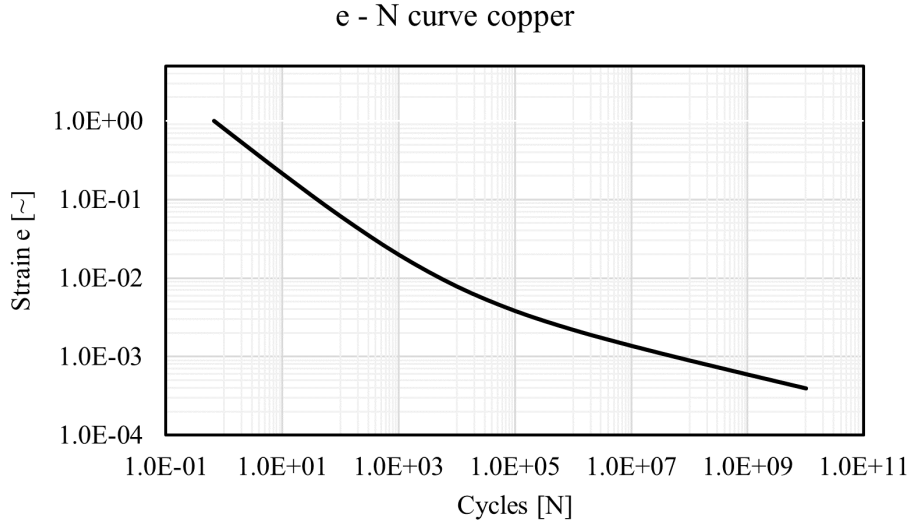

Figure 17: ϵ-N copper curve [18].

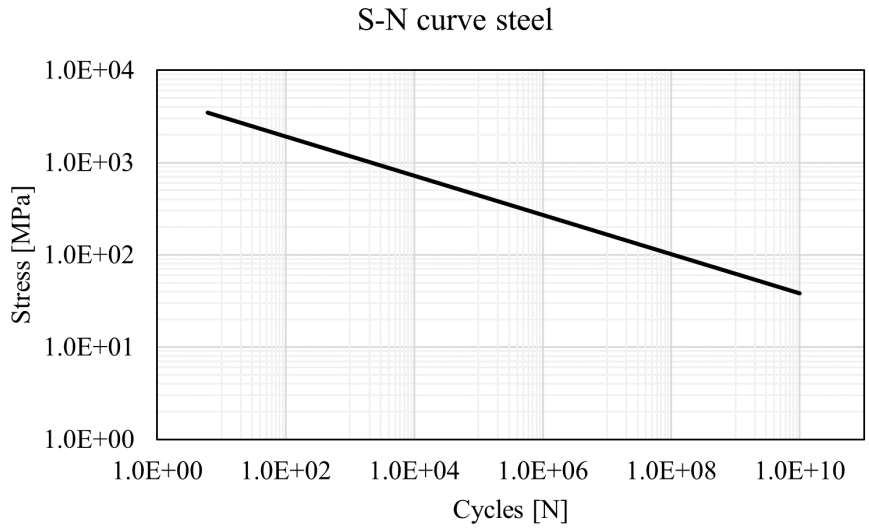

Figure 18: S-N steel curve [7].

3.6.3. Damage estimation

For each component, the number of cycles is counted using the rain flow counting method [22]. Later, fatigue life is estimated using the Palmgren–Miner rule of damage accumulation [28]. The cumulative damage overall (Eq. 26) represents the aggregation of each individual damage fraction. When $D = 1$, it indicates that the structure has reached its fatigue life limit and may fail. In contrast, if $D < 1$, it suggests that the structure still has some remaining life.

$$D = \sum_{i=1}^{n} \left(\frac{n_i}{Ncycles} \right) \tag{26}$$

4. QUASI-STATIC CABLE MODEL

The method of integrating a static cable model into a dynamic simulation is referred to as the **quasi static (QS)** approach. In this type of analysis, after performing the dynamic simulation, the positions of both the HOP and the **anchor point (AP)** are identified. These positions are then used in the static cable model to determine the force distribution. Such models serve as good approximations for the preliminary design of the umbilical power cable. It should be noted that this model does not consider hydrodynamic forces and bending stiffness, it only considers the **submerged weight** (ω) (buoyancy - weight) of each section and the axial stiffness.

4.1. Mathematical model

The problem is simplified as 2D, and, as mentioned above, the external forces considered for this analysis are the weight cable, the buoyancy of the cable and the buoyancy produced by the floating modules. To develop this model, the cable is divided into three sections. The catenary equation for each section is formulated independently and then the problem is addressed by applying the static equilibrium of the whole umbilical cable.

4.1.1. Elastic catenary

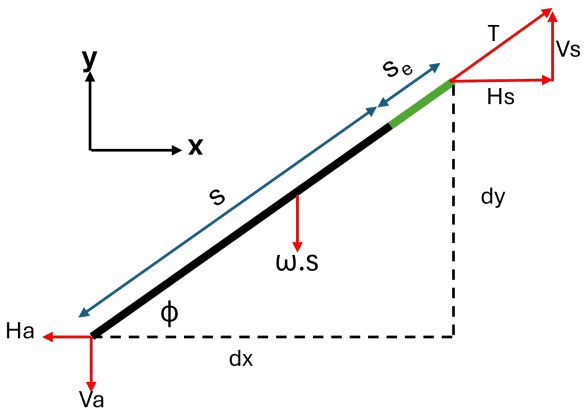

Figure 19: Equilibrium of an elastic catenary segment for QS model.

In an elastic catenary, the cable is replaced by a spring that can stretch in response to tension. The spring is assumed to stretch in accordance with Hooke's law. Specifically, if s is the natural length of a section of spring, then the spring length with the applied tension T has length:

$$s_t = s + s_e = s\left(1 + \frac{T}{EA}\right)$$

where EA is the axial stiffness of the cable. In the catenary the value of T is variable, but the ratio remains valid at a local level, so

$$\frac{ds_t}{ds} = 1 + \frac{T}{EA}$$

The equations for the cable tension at the point s are: $V_s = T\cos(\phi)$ and $H_s = T\sin(\phi)$. Then considering that the variation dy/dx can be approximated as the tangent of the angle formed by the forces V_s and H_s, it gives the following expressions.

$$\frac{dy}{dx} = \tan(\phi) = \frac{V_s}{H_s}, T = \sqrt{{H_s}^2 + {V_s}^2}$$

$$\frac{dx}{dst} = \cos(\phi) = \frac{H_s}{T}$$

$$\frac{dy}{dst} = \sin\phi = \frac{V_s}{T}$$

The variation dx and dy can be expressed in terms of the natural length according to:

$$\frac{dx}{ds} = \frac{dx}{dst}\frac{dst}{ds} = \frac{H_s}{T} \cdot \left(1 + \frac{T}{EA}\right)$$

$$\frac{dy}{ds} = \frac{dy}{dst}\frac{dst}{ds} = \frac{V_s}{T} \cdot \left(1 + \frac{T}{EA}\right)$$

The coordinates x(s) and y(s) for every point of the cable result from the integration of the previous expressions. The integration is made by parts, and a change of variable to pass from ds to dVs is needed to simplify expressions. Based on the equilibrium of the system, the vertical force at position s is given by $V_s = V_a + \omega s$ when the distributed weight acts downward and by $V_s = V_a - \omega s$ when it acts upward. In contrast, the horizontal force H_s remains constant due to the absence of any other horizontal forces acting on the cable.

$$x = \int \left(\frac{H_s}{T}\right) ds + \int \left(\frac{H_s}{EA}\right) ds$$

$$y = \int \left(\frac{V_s}{T}\right) ds + \int \left(\frac{V_s}{EA}\right) ds$$

Distributed weight acts downwards.

$$Vs = Va + \omega s, ds = \frac{dVs}{\omega}$$

Integration for the horizontal position (x)

$$\int \left(\frac{H_s}{T}\right) ds = \int \left(\frac{H_s}{\sqrt{{H_s}^2 + {V_s}^2}}\right) ds = \frac{H_s}{\omega} \int \left(\frac{1}{\sqrt{1 + \left(\frac{V_s}{H_s}\right)^2}}\right) d(Vs/Hs)$$

$$\int \left(\frac{H_s}{T}\right) ds = \frac{H_s}{\omega} \left[\arcsin \frac{V_s}{H_s}\right]_{Va}^{Vs}$$

$$\int \left(\frac{H_s}{EA}\right) ds = \left[\frac{H_s \cdot s}{EA}\right]_0^s$$

$$x = \frac{H_s}{\omega} \left[\arcsin \frac{V_s}{H_s}\right]_{Va}^{Vs} + \left[\frac{H_s \cdot s}{EA}\right]_0^s \tag{27}$$

Integration for the vertical position (y)

$$\int \left(\frac{V_s}{T}\right) ds = \int \left(\frac{V_s}{\sqrt{{H_s}^2 + {V_s}^2}}\right) ds = \frac{1}{2\omega} \int \left(\frac{1}{\sqrt{{H_s}^2 + {V_s}^2}}\right) (2Vs) dVs$$

$$\int \left(\frac{V_s}{T}\right) ds = \frac{H_s}{\omega} \left[\sqrt{1 + \left(\frac{Vs}{Hs}\right)^2}\right]_{V_a}^{Vs}$$

$$\int \left(\frac{V_s}{EA}\right) ds = \int (Va + \omega s)\, ds = \left[V_a s + \frac{\omega s^2}{2}\right]_0^s$$

$$y = \frac{H_s}{\omega} \left[\sqrt{1 + \left(\frac{Vs}{Hs}\right)^2}\right]_{Va}^{Vs} + \left[V_a s + \frac{\omega s^2}{2}\right]_0^s \tag{28}$$

Distributed weight acts upwards.

$$Vs = Va - \omega s, ds = \frac{-dVs}{\omega}$$

Integration for the horizontal position (x)

$$\int \left(\frac{H_s}{T}\right) ds = \int \left(\frac{H_s}{\sqrt{{H_s}^2 + {V_s}^2}}\right) ds = -\frac{H_s}{\omega} \int \left(\frac{1}{\sqrt{1 + \left(\frac{V_s}{H_s}\right)^2}}\right) d(Vs/Hs)$$

$$\int \left(\frac{H_s}{T}\right) ds = -\frac{H_s}{\omega} \left[\arcsin \frac{V_s}{H_s}\right]_{Va}^{Vs}$$

$$\int \left(\frac{H_s}{EA}\right) ds = \left[\frac{H_s \cdot s}{EA}\right]_0^s$$

$$x = -\frac{H_s}{\omega}\left[\arcsin\frac{V_s}{H_s}\right]_{Va}^{Vs} + \left[\frac{H_s \cdot s}{EA}\right]_0^s \tag{29}$$

Integration for vertical position (y)

$$\int\left(\frac{V_s}{T}\right)ds = \int\left(\frac{V_s}{\sqrt{{H_s}^2 + {V_s}^2}}\right)ds = -\frac{1}{2\omega}\int\left(\frac{1}{\sqrt{{H_s}^2 + {V_s}^2}}\right)(2Vs)dVs$$

$$\int\left(\frac{V_s}{T}\right)ds = -\frac{H_s}{\omega}\left[\sqrt{1+\left(\frac{Vs}{Hs}\right)^2}\right]_{Va}^{Vs}$$

$$\int\left(\frac{V_s}{EA}\right)ds = \int(Va - \omega s)\,ds = \left[V_a s - \frac{\omega s^2}{2}\right]_0^s$$

$$y = -\frac{H_s}{\omega}\left[\sqrt{1+\left(\frac{Vs}{Hs}\right)^2}\right]_{Va}^{Vs} + \left[V_a s - \frac{\omega s^2}{2}\right]_0^s \tag{30}$$

In the process of modeling the DPC, the distributed weight exerts a downward force in the sagging and dragging regions (Eqs. 27, 28), and an upward force in the buoyant region (Eqs. 29, 30).

4.1.2. Free body diagram

The initial segment (drag segment S_c) extends from the **anchor point (AP)** to the point **p**. The subsequent segment (buoyancy segment S_b) continues from point **p** to point **q**. Lastly, the final segment (sagging segment S_c) extends from point **q** to the **hang-off point (HOP)** (Fig. 20).

The equations to describe the shape of a catenary are deduced in (Sec. 4.1.1), this method uses the length of the cable (**s**), the axial stiffness (**EA**), and the forces at its ends (**V, H**) to describe the catenary as parametric functions of length ($x(s)$ **&** $z(s)$)

The mechanical properties of the cable remain unchanged because we are considering a single continuous cable. However, the submerged weight in the buoyancy section (ω_b) is different from the sagging and dragging section (ω_c, ω_a) due to the increased buoyancy provided by the floaters.

4.1.3. Drag section

To evaluate the positions x and z along the length of the cable, the expressions described in (Eqs. 31, 34) are used. The cable analysis is split in three section (Fig. 21), non active

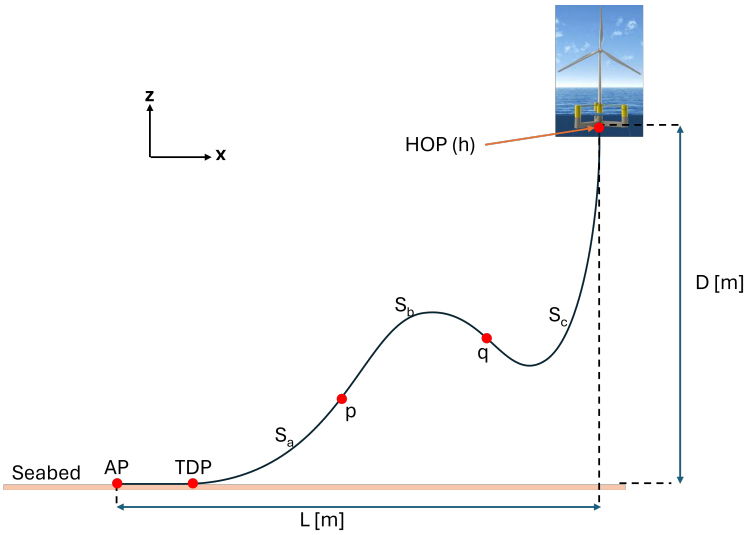

Figure 20: DPC Initial configuration for QS model.

length form AP to x_0, frictional length from x_0 to TDP (L_B), and finally the hanging length from the TDP to the start of the buoyancy section (point p):

- From AP to x_0: This section is not affected by the horizontal tension of the cable and is free resting on the seabed.
- From x_o to L_B: This segment experiences seabed friction, calculated as $Fr = C_B \cdot (TDP - L_B)$, where C_B is the friction coefficient measured in [N/m]. A sufficient amount of friction force is generated, from x_0 to L_B, to balance the horizontal tension at the point p (H_p).
- From L_B until the end S_a: This hanging section is affected by its own weight, and the sum of the suspended weight must be in the same vertical tension at the point p (V_p).

$$x(s) = \begin{cases} s & \text{for } 0 \leq s < s_{z0} \\ s + \frac{C_B \omega_a}{2EA}(s^2 - 2x_0 s + x_0 \lambda) & \text{for } x_0 \leq s < L_B \\ L_B + \frac{H}{\omega_a} \ln \left[\frac{\omega_a (s - L_B)}{H} + \sqrt{1 + \left(\frac{\omega_a (s - L_B)}{H} \right)^2} 1 \right] + \frac{Hs}{EA} + \frac{C_B \omega_a}{2EA} \left[x_0 \lambda - L_B^2 \right], & \text{for } L_B \leq s < L \end{cases} \tag{31}$$

where λ is:

$$\lambda = \begin{cases} \frac{L_B - H}{C_B \omega_a}, & \text{if } x_0 > 0 \\ 0, & \text{otherwise} \end{cases} \tag{32}$$

$$\omega_a = (\gamma - A \cdot \rho) \cdot g \tag{33}$$

γ is the linear density of the cable, ρ is the sea water density (1025 $[kg/m^3]$), and g is the gravity acceleration (9.80665 $[m/s]$).

In the expression for $z(s)$ the elevation beyond L_B is zero, since the line rests on the seabed and forces only occur parallel to the horizontal plane (Eq. 34).

$$z(s) = \begin{cases} 0 & \text{if } 0 \leq s \leq L_B \\ \frac{H}{\omega}\left[\sqrt{1+\left(\frac{w(s-L_B)}{H}\right)^2}-1\right], & \text{if } L_B < s \leq L \end{cases} \tag{34}$$

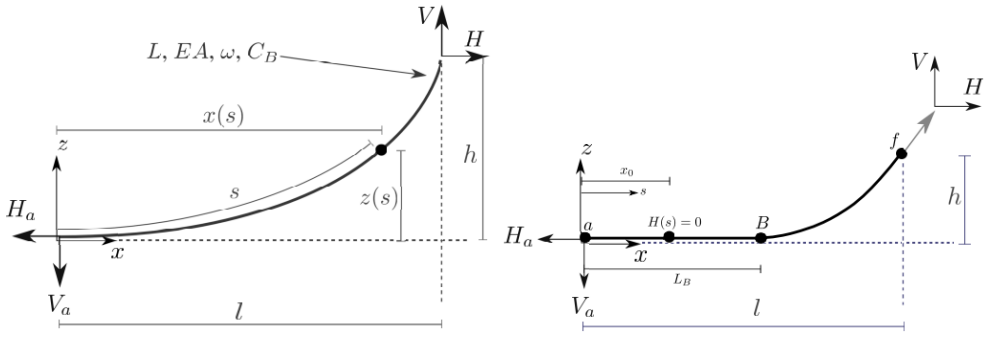

(a) Single line cable element suspended in fluid and anchored to the seabed. **(b)** Single line cable resting on the seabed and anchored to the seabed.

Figure 21: Drag section cable segmentation [21].

From the evaluation of $x(s)$ and $z(s)$ at the point p, the variations in x and z (Δ_x and Δ_z) for the drag section are estimated. At point AP (a), both x (x_a) and z (z_a) are zero. The unknowns in these two new equations (Eqs. 35, 36) are the vertical and horizontal forces V_p **and** H_p, and its coordinates x_p, z_p.

$$x_p - x_a = S_a - \frac{V_p}{\omega_a} + \frac{V_p}{\omega_a} ln\left[\frac{V_p}{H_p} + \sqrt{1+\left(\frac{V_p}{H_p}\right)^2}\right] + \frac{H_p}{EA} + \frac{C_B \times \omega_a}{2AE}\left[-\left(S_a - \frac{V_p}{\omega_a}\right) + \left(S_a - \frac{V_p}{\omega_a} - \frac{H_p}{C_B\omega_a}\right) MAX\left(S_a - \frac{V_p}{\omega_a} - \frac{H_p}{C_B\omega_a}\right)\right] \tag{35}$$

$$z_p - z_a = \frac{H_p}{\omega_a}\left[\sqrt{1+\left(\frac{V_p}{H_p}\right)^2}-1\right] + \frac{{V_p}^2}{2EA\omega_a} \tag{36}$$

The unknown variables from this cable segment are: x_p, z_p, H_p, V_p.
The known variables from this cable segment are: x_a, z_a.

4.1.4. Buoyancy section

The equations that define the horizontal and vertical coordinates within the buoyancy section are given by (Eq. 37 and Eq. 38), starting from point (p). Similarly to the previous section, these coordinates are evaluated at (q), considering the variations in weight and buoyancy throughout its length.

$$x(s) = x_p + \frac{H_p}{\omega_b}\left\{\ln\left[\frac{V_p}{H_p} + \sqrt{1+\left(\frac{V_p}{H_p}\right)^2}\right] - \ln\left[\frac{V_p-\omega s}{H_p} + \sqrt{1+\left(\frac{V_p-\omega s}{H_p}\right)^2}\right]\right\} + \frac{Hs}{EA} \tag{37}$$

$$z(s) = z_p + \frac{H_p}{\omega b}\left[\sqrt{1+\left(\frac{V_p}{H_p}\right)^2} - \sqrt{1+\left(\frac{V_p-\omega s}{H_p}\right)^2}\right] + \frac{1}{EA}\left(V_p s - \frac{\omega_b s^2}{2}\right) \tag{38}$$

The submerged weight of the buoyancy section (ω_b) is estimated as the submerged weight of the cable (ω_a) plus the contribution of the buoyancy of the floaters (Eq. 39). where N_f is the number of floaters and B_f is the buoyancy produced by one floater, and S_b is the length of the buoyancy segment.

$$\omega_b = N_f \cdot B_f / S_B - \omega_a \tag{39}$$

The vertical force at (p) is incremented by the buoyancy effect $V_p = V_q + \omega_b S_B$ and $s = S_b$, then replacing this into (Eq. 37 and Eq. 38) the changes in horizontal position Δ_x and height Δ_z are estimated.

$$x_q - x_p = \frac{H_q}{\omega_b}\left\{ln\left[\frac{V_q + S_B\,\omega_b}{H_q} + \sqrt{\frac{(V_q + S_B\,\omega_b)^2}{{H_q}^2} + 1}\right] - ln\left[\frac{V_q}{H_q} + \sqrt{\frac{{V_q}^2}{{H_q}^2} + 1}\right]\right\} + \frac{H_q\,S_B}{AE} \tag{40}$$

$$z_p - z_q = \frac{H_q}{\omega_b}\left[\sqrt{1+\left(\frac{V_q + w_b S_B}{H_q}\right)^2} - \sqrt{1+\left(\frac{V_q}{H_q}\right)^2}\right] + \frac{1}{AE}\left(V_q S_B + \frac{\omega_b S_B}{2}\right) \tag{41}$$

The main difference between this section and the other two sections is that the net weight has an upward direction, creating a positive net force that lifts the cable (Appx. 4.1.1).

The equilibrium es estimated between the point (p) and the HOP (Fig. 22), the sum of the vertical forced included the distributed weight in the buoyancy and the sagging section (Eq. 42), on the other hand the horizontal remains constant (Eq. 43).

$$V_h - \omega_c \cdot S_c + \omega_b \cdot S_b - V_p = 0 \tag{42}$$

$$H_h - H_p = 0 \tag{43}$$

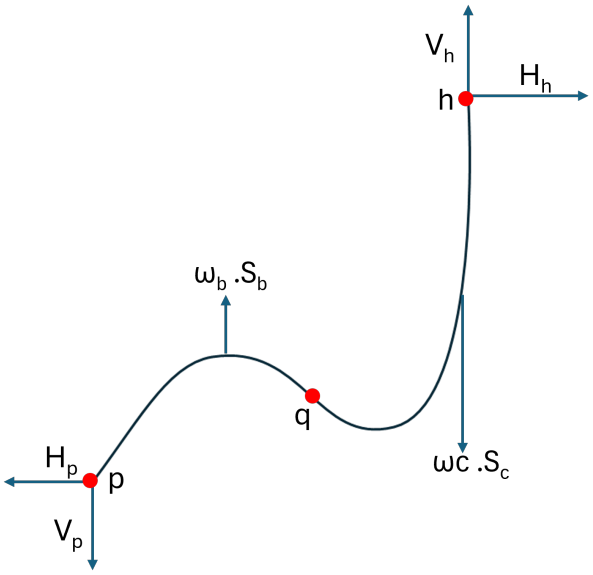

Figure 22: Balance of forces including buoyancy and sagging sections.

The unknown variables from this cable segment are: x_p, z_p, x_q, z_q, H_p, V_p, H_h, V_h.

4.1.5. Sagging section

The expressions to estimate the vertical and horizontal positions of the catenary are given by (Eq. 44 and Eq. 45),the unknowns are the vertical and horizontal forces at q (V_q and H_q).

$$x(s) = x_q + \frac{H_q}{\omega_c}\left\{ln\left[\frac{V_q+\omega_c s}{H_q}+\sqrt{1+\left(\frac{V_q+\omega_c s}{H_q}\right)^2}\right]-ln\left[\frac{V_q}{H_q}+\sqrt{1+\left(\frac{V_q}{H_q}\right)^2}\right]\right\}\frac{H_s}{EA} \tag{44}$$

$$z(s) = z_q + \frac{H_q}{\omega_c}\left[\sqrt{1+\left(\frac{V_q+\omega_c s}{H_q}\right)^2}-\sqrt{1+\left(\frac{V_q}{H_q}\right)^2}\right]+\frac{1}{EA}\left(V_q s+\frac{\omega_c s^2}{2}\right) \tag{45}$$

$$\omega_c = \omega_a \tag{46}$$

Then to express these equation by the variables at the point HOP (h), the vertical force (V_q) and the arc length (s) can be written as:

$$V_q = V_h - \omega_c S_c \tag{47}$$

$$s = S_c \tag{48}$$

By substitution of (Eq. 48 and Eq. 47) into (Eq.44 and Eq.45), The changes in horizontal position Δ_x and height Δ_z are estimated according to the following equations:

$$x_h - x_q = \frac{H_q}{\omega_c}\left\{ln\left[\frac{V_h}{H_q} + \sqrt{1+\left(\frac{V_h}{H_q}\right)^2}\right] - ln\left[\frac{V_h - \omega_c S_c}{H_q} + \sqrt{1+\left(\frac{V_h - \omega_c S_c}{H_q}\right)^2}\right]\right\} + \frac{H_q S_c}{EA} \tag{49}$$

$$z_h - z_q = \frac{H_q}{\omega_c}\left[\sqrt{1+\left(\frac{V_h}{H_q}\right)^2} - \sqrt{1+\left(\frac{V_h - \omega_c S_c}{H_q}\right)^2}\right] + \frac{1}{EA}\left(V_h S_c - \frac{\omega_c S_c^2}{2}\right) \tag{50}$$

The reader must keep in mind that the catenary equations are developed for each section separately, on the other hand, the equilibrium equations start from the platform and go all the way down until the point P. as shown in Fig. 23 and Fig. 22

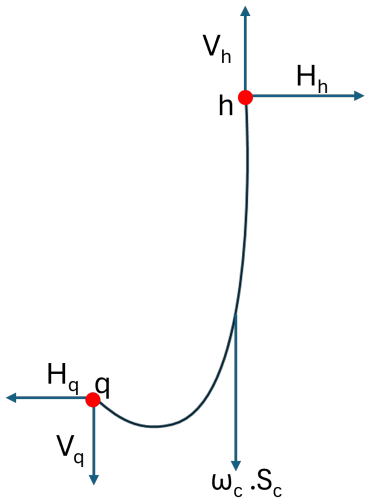

Figure 23: Balance of forces for sagging section.

The balance equations required for this cable section to remain in equilibrium are:

$$V_h - \omega_c \cdot S_c - V_q = 0 \tag{51}$$

$$H_h - H_q = 0 \tag{52}$$

The unknown variables from this cable segment are: x_q, z_q, H_q, V_q.
The known variables from this cable segment are: z_h, z_h.

4.1.6. System assembly

The mathematical model (Eq. 53) that describes the cable configuration is a problem bounded by 10×10. This system is highly non-linear and can be expressed as $F(x) = B$, where B is the boundary condition matrix. For simplicity, all equations are represented in the form $f_i(x) - b_i = 0$.

$$[(Eq.35), (Eq.36), (Eq.49), (Eq.50), (Eq.40), (Eq.41), (Eq.52), (Eq.51), (Eq.43), (Eq.42)]' \tag{53}$$

The unknown variables for the DPC are: x_p, z_p, H_p, V_p, x_q, z_q, H_q, V_q, H_h, V_h
The known variables (boundary conditions) for the DPC are: x_a, z_a, x_h, z_h

The system is solved using the MATLAB function **fsolve** (Eq. 54), which is useful for solving non-linear systems.

$$W = fsolve(F_{system}(X), X0) \tag{54}$$

Where W is the solution given the boundary conditions (x_a, z_a, x_h, z_h), F_{system} is the equation system (Eq. 53) that represents the DPC, X contains the variables of the system ($X = [H_h, V_h, H_p, V_p, x_p, z_p, H_q, V_q, xq, z\text{q}]$), and X0 is the initial guess.

4.2. Static equilibrium

In this section, the curvature and effective tension are calculated and represented as functions of the length of the cable for easy comparison.

The same cable (Tab. 12) is modeled in OrcaFlex (FEM model); in this case, axial stiffness, bending stiffness, and torsional stiffness are included. The length of the sections is Sa = 93.77 [m], Sb = 60.68 [m], Sc = 129.45 [m], L 150 [m], D 186 [m]. The floaters are introduced as discrete points every 2 [m] along the buoyancy section; finally the cable is considered to be clamped at both ends, which means the cable is perpendicular to the platform at andA (HOP) and parallel to the seabed and endB (AP). In the FEM model, no additional forces coming from wave elevation, current, or platform motion are considered.

The lazy wave profile resulting after solving the system non-linear system of equations (Eq.53) for the QS model is illustrated in (Fig. 24). The differences between QS and OrcaFlex at the point (p) for the horizontal and vertical coordinates $x(s)$ and $z(s)$, are 0.4% and 0.0% respectively, while at the point (q) they are 0.5% and 0.4% respectively.

This indicates that the QS model can be a good approximation to analyze static equilibrium.

The configuration of the sections of the cable are; Sa=93.77[m], Sb = 60.68[m], Sc=129.45[m], L 150[m], D 186[m].

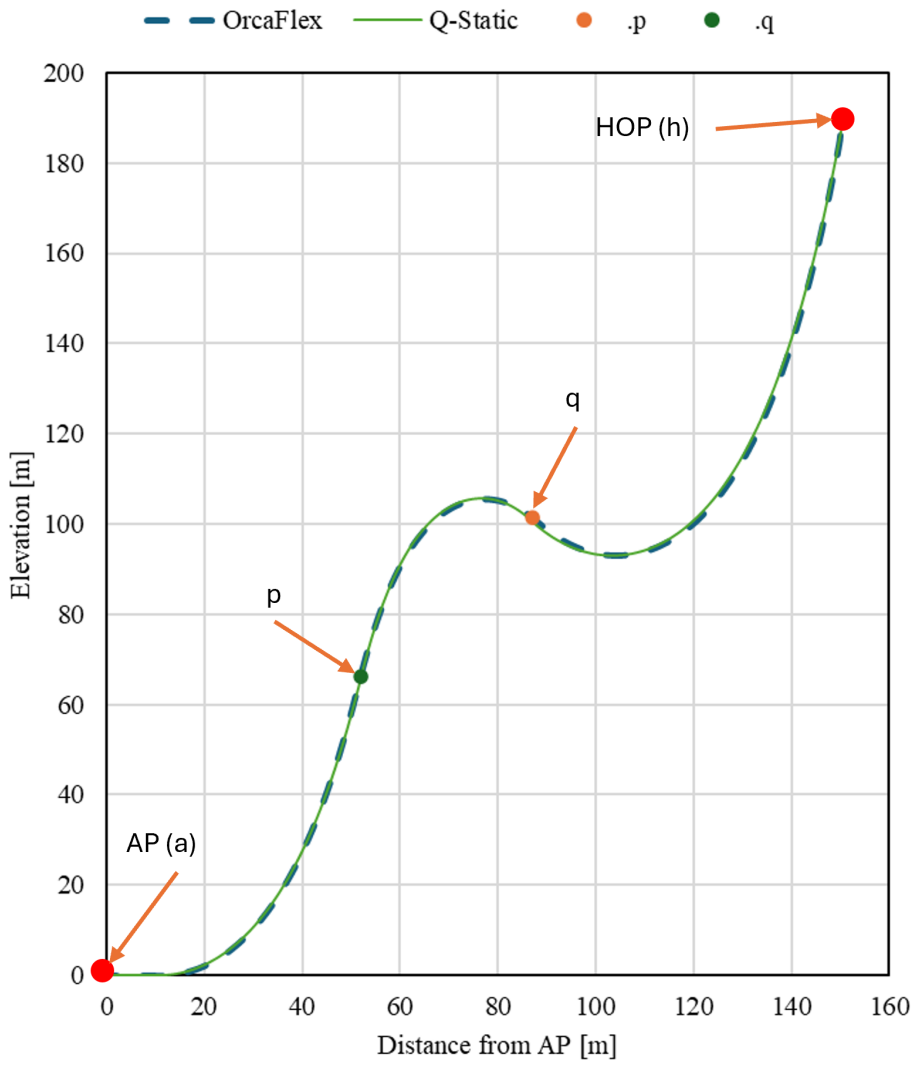

Figure 24: Dynamic power cable profile for QS and FEM models.

4.2.1. Curvature

Based on [6], every differentiable curve can be parameterized with respect to the length of the arc. In the case of a plane curve, this means the existence of a parameterization γ (s) = (x (s), y (s)), where x and y are differentiable functions with real values whose derivatives satisfy

$$\|\gamma'\| = \sqrt{x'(s)^2 + z'(s)^2} = 1 \tag{55}$$

If the curve is twice differentiable, that is, if the second derivatives of x and y exist, the curvature can be estimated as:

$$k(s) = \sqrt{x''(s)^2 + z''(s)^2} \tag{56}$$

According to the formulation in [6], we evaluate the curvature (Eq.56) for the QS. It is crucial to note that the second derivative should be calculated for each individual section. Moreover, the curvature between AP and TDP is zero because there is no $z(s)$ elevation; the cable lies on the seabed.

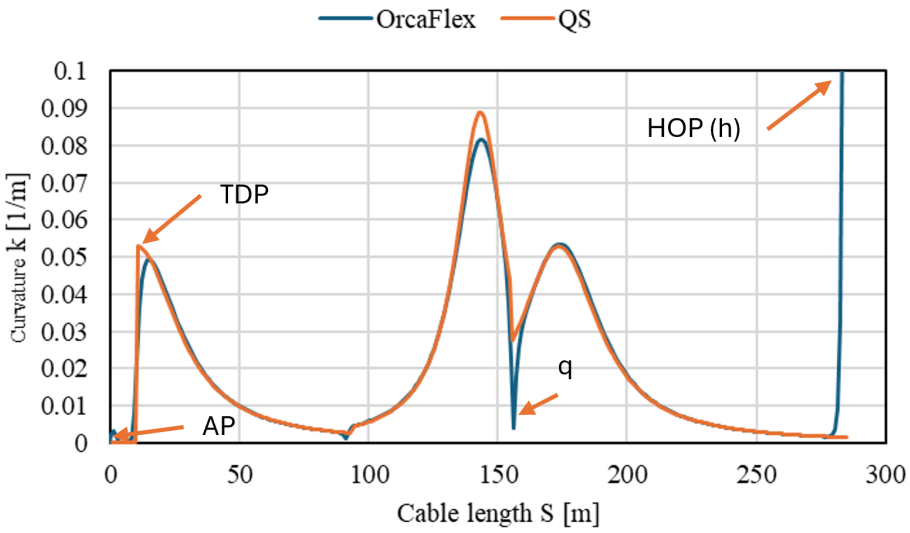

Figure 25: Curvature comparison between QS and FEM models.

There are some regions where the QS model results differ from those obtained from Orcaflex (Fig. 25).

- In the AP: Because the OrcaFlex model allows some penetration in the seabed, there is a change in the curvature form from AP to TDP different from zero.
- In the TDP: Compared to the QS model, the OrcaFlex results show a smooth transition between the cable laying on the seabed and the hanging cable; this might be due to the inclusion of bending stiffness. further analysis will be necessary at this zone.
- The third peak is located in the buoyancy section: in OrcaFlex the floaters are modeled as discrete points along the section. Replacing this section by a new type of cable that includes the buoyancy of the floaters as part of its properties might mitigate this problem.
- Point p: the QS model ensures only the continuity of vertical and horizontal forces at the points p and q, on the other hand OrcaFlex ensures a smooth transition in

curvature because it considers the bending stiffness.

- At HOP: the reason for the highest curvature at this point is because the cable is clamped at this end, producing a big change in curvature to reach perpendicular to the platform.

4.2.2. Effective tension

The horizontal tension is constant for all sections, except where the cable rests on the seabed, but the vertical tension changes along the cable to balance the weight of the suspended cable. In the (QS) the vertical tension at the anchor point is zero, and the effective tension is constant until the cable stars to elevate producing a vertical component force in the z direction.

The **effective tension (Te)** is calculated as the contribution of the horizontal and vertical tension (Eq. 57). Due to the fact that the catenary equations for each section were formulated independently, Te is estimated following the expression for each section described in (Eq.58).

$$Te = \sqrt{H_s^2 + V_s^2} \tag{57}$$

$$Te(s) = \begin{cases} H & \text{for } 0 \leq s < L_B \\ \sqrt{H^2 + ((s - L_{seabed}) \cdot \omega_a)^2} & \text{for } L_B \leq s < S_A \\ \sqrt{H^2 + (V_p - s \cdot \omega_b)^2}, & \text{for } 0 \leq s < S_B \\ \sqrt{H^2 + (V_q + s \cdot \omega_c)^2}, & \text{for } 0 \leq s < S_C \end{cases} \tag{58}$$

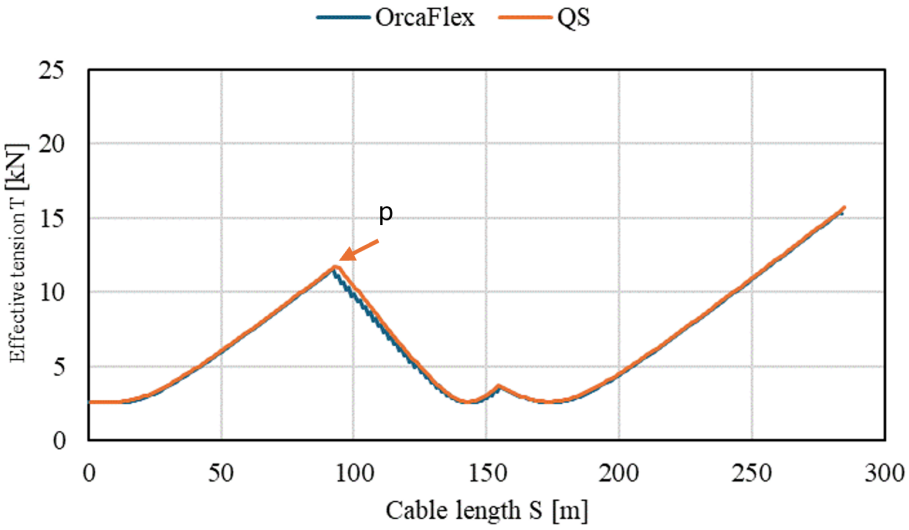

Figure 26: Effective tension comparison between QS and FEM models.

The distribution of effective tension (Fig. 26) is more accurate, only a small variation is found at the point p; the rest of the cable matches the results obtained in OrcaFlex.

4.3. Fatigue analysis

Under normal operating conditions, the probable sea states are detailed in (Table 5). In this section, only the response to STSS16 is analyzed; this case represents the most extreme load scenario in a short-term sea state analysis.

Once the effective tension and curvature curves have been determined, the method described in (Section 3.6.1) is used to estimate the stress developed in the cable.
The dynamic simulation is divided into two stages, one to let the system start and, and the second is itself the simulation for data analysis. Stage 1 lasts 7 minutes, and stage 2 has a duration of 1 hour thus because only one STSS is considered.

In fatigue analysis, stresses are evaluated at locations $.p$ and $.q$ for each stationary point of the horizontal platform‘s position. Following this, the load cycles are identified using the rain flow counting method described in [22], and the damage is assessed based on the Palmgren-Miner damage accumulation principle outlined in (Section 3.6.3).

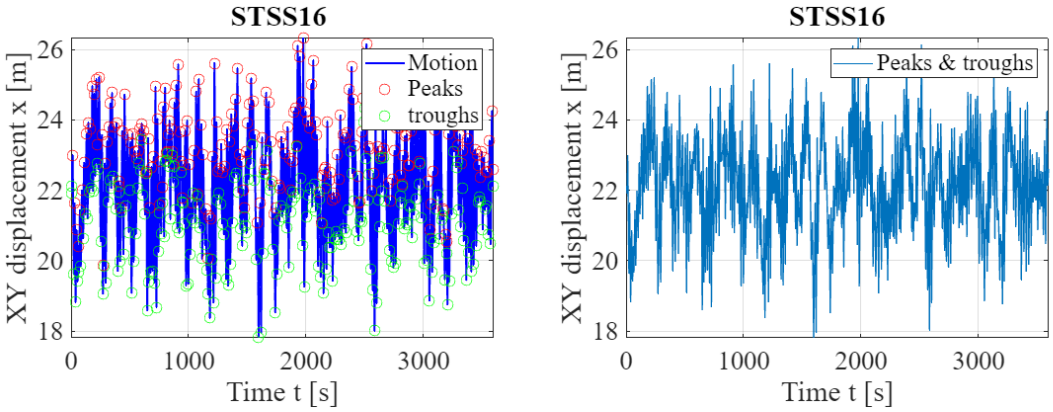

(a) XY Excursion from the origin. **(b)** Peaks and troughs.

Figure 27: Excursion of the VolturnUS-S platform under the STSS16 1-hour load condition.

It is crucial to note that the QS is not solved for every time step of the horizontal position of the platform. Instead, the non-linear problem (Eq. 53) is only solved at the peaks and troughs generated during the horizontal movement while operating STSS16.

4.3.1. Rain-Flow counting

The Rain-flow counting method is utilized to transform a sequence of fluctuating stress into a collection of constant amplitude stresses with defined occurrences [22], it is applied in fatigue analysis when the load magnitudes are variable. The results for points p and q are illustrated in (Figs. 28, 29).

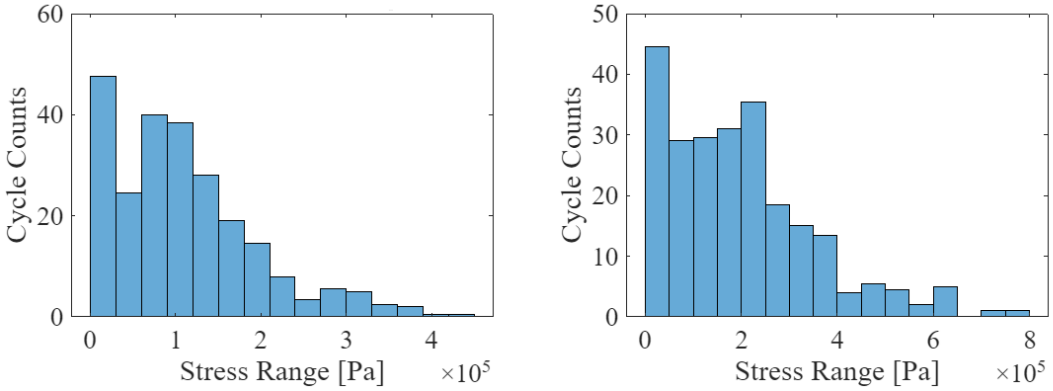

(a) Armour **(b)** Conductor

Figure 28: Rain-Flow counting at point p.

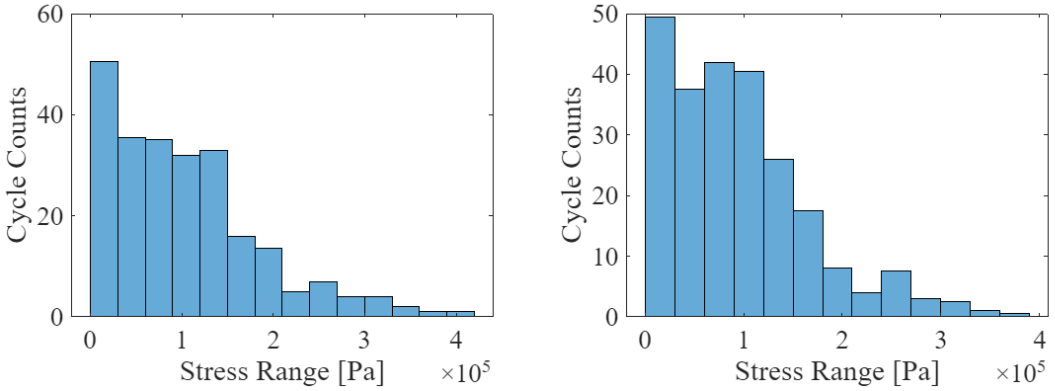

(a) Armour **(b)** Conductor

Figure 29: Rain-Flow counting at point q.

4.3.2. Life estimation along the cable

When estimation the fatigue life of the cable, the QS does not produce accurate results. At some points the fatigue obtained with the quasi-static model matches the results from OrcaFlex, and the rest of the curve deviates from the FEM results, one of the main causes could be that inertial and viscous forces are not included in the QS model. The outcomes from the quasi-static model are commented hereby.

Curvature

The curvature is the critical variable when using the QS to perform a fatigue analysis. At some points of the cable the curvature has small variations during the simulation resulting in a longer fatigue life, these points correspond to the section where the maximum (QS Maximum) and minimum (QS Maximum) curves pass through the same points (QS Mean) (Fig. 30). Furthermore, the fluctuation in curvature predicted by the QS model is less significant compared to that obtained using OrcaFlex. Except for the TDP, in the rest of the cable the curves predicted by the QS model approximate the average values (OrcaFlex Mean) obtained from OrcaFlex.

Effective tension

Similar to the curvature curves, the tension curves estimated using the QS have small variation. In the vicinity of the TDP (left side of Fig. 31), the tension estimated using the QS model is close to the minimum values recorded in OrcaFlex. However, for the remainder of the cable, these estimates tend to align with the mean values from OrcaFlex. It should be noted that all the values derived from the QS model fall within the maximum and minimum range obtained from OrcaFlex (Fig. 31).

Stress estimation

The stress distributions for the conductor and armour are highly affected by the curvature distribution (Fig. 32). This distribution is highly dependent on the stress factors presented

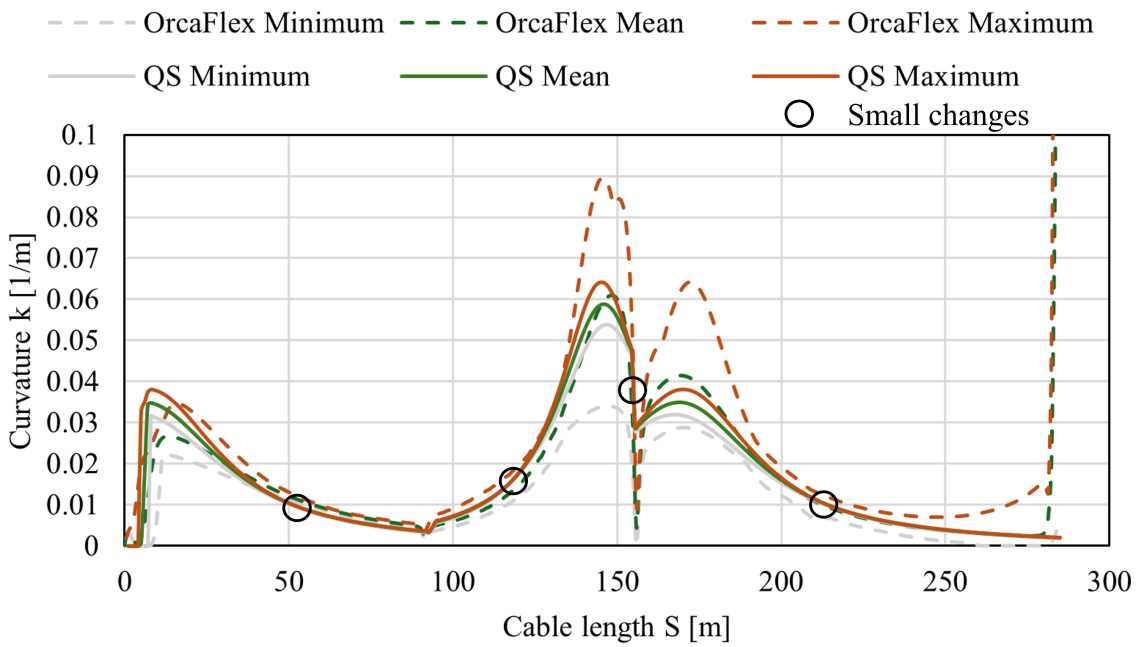

Figure 30: Curvature variation for 1[h] simulation time of STSS16.

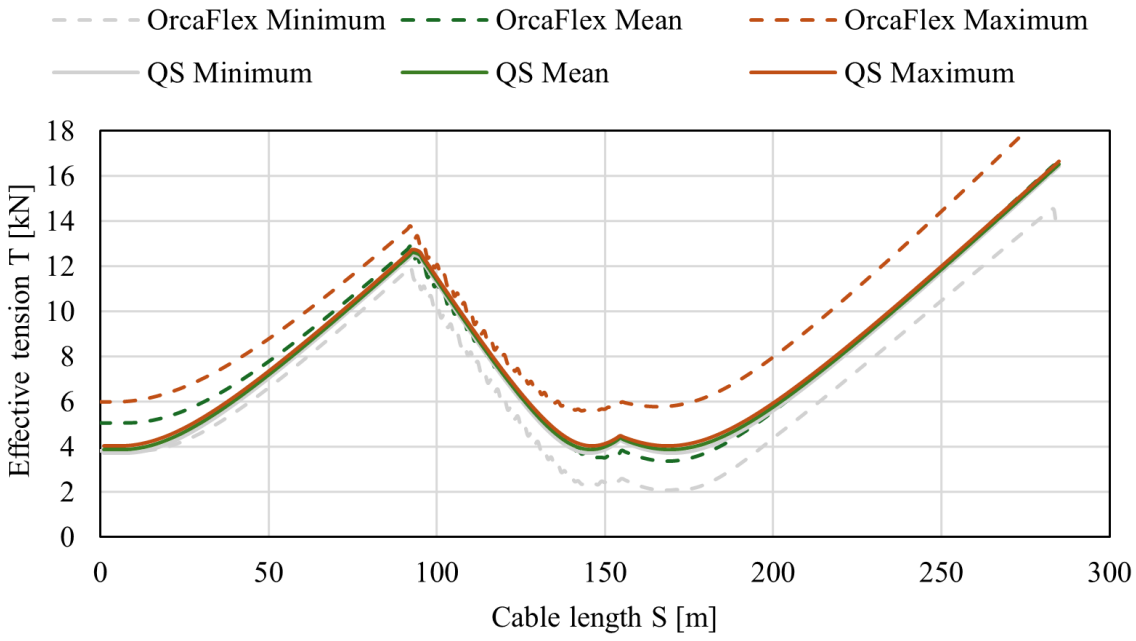

Figure 31: Effective tension variation for 1[h] simulation time of STSS16.

in **Chapter 3**, since the stress factors for the curvature are too large compared to the stress factors for the tension (see Table 9), the profile of the stresses developed in the cable will follow the curvature; Indeed, the drawback of the curvature variation will influence these curves.

The stress distributions are shown in Fig. 32, (a) illustrates the stress distribution for the armour and (b) depicts the stress distribution for the conductor. The presence of regions where stress remains unchanged (areas within circles) results in a longer lifespan because fatigue is caused by fluctuations in stress, and in these regions, the fluctuations are minimal.

These areas correspond to the four peaks illustrated in Fig. 33. The estimated fatigue life in these regions is longer compared to the OrcaFlex results.

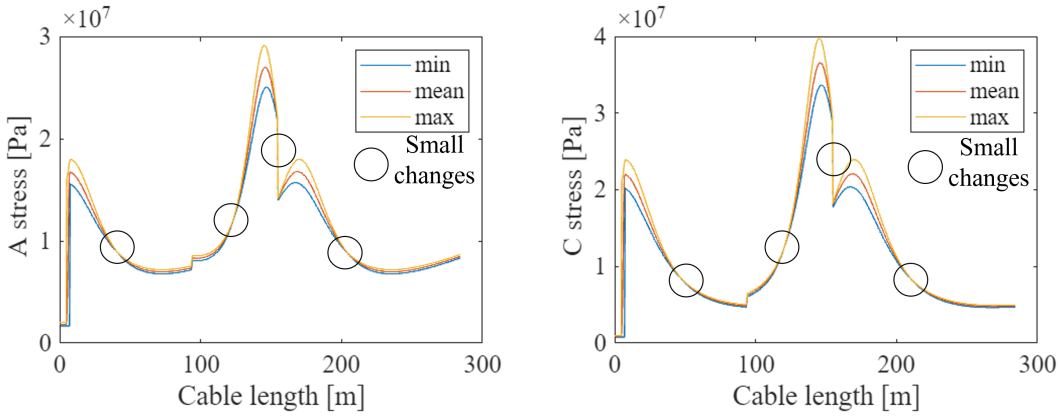

(a) Armour stress **(b)** Conductor stress

Figure 32: Stress estimation in cables using the stress factors method for the QS model..

Life estimation

In the previous section of this chapter the data correspond to the simulation time of 1 [h], to estimate the fatigue life of the cable in years, it is assumed that STSS16 occurs every day for 365 days.

In both models the armour fails first, the lowest registered values with the QS model are located in the TDP (left side of Fig. 33) and in the HOP with the OrcaFlex model (Fig. 33), In the QS curves, four peaks indicate areas where fatigue life is considerably extended, resulting from the constant stress zones in the cable throughout the simulation.

The HOP is the area of the cable most likely to experience stress concentration because it is modeled as clamped to the platform, the results from Orcaflex indicates 6 years for the conductor and 92 years for the armour at his location, given that the sea is depicted using only the STSS 16. The QS model does not accurately represent these values; it may be necessary to analyze this section as a clamped beam rather than as a cable connected to a pin (as in the current model).

The QS model introduced in this section is a good tool for estimating the distribution of internal forces for static analysis. In fatigue, this model can be used to make a comparison between two cables during the initial design stage of the system. However, when fatigue analysis is performed, the omission of inertial and damping forces could lead to inaccurate results.

For a final design, it is recommended to validate the configuration of the riser system with some FEM model to include all the forces acting on the cable, such as OrcaFlex, Moordyn, etc.

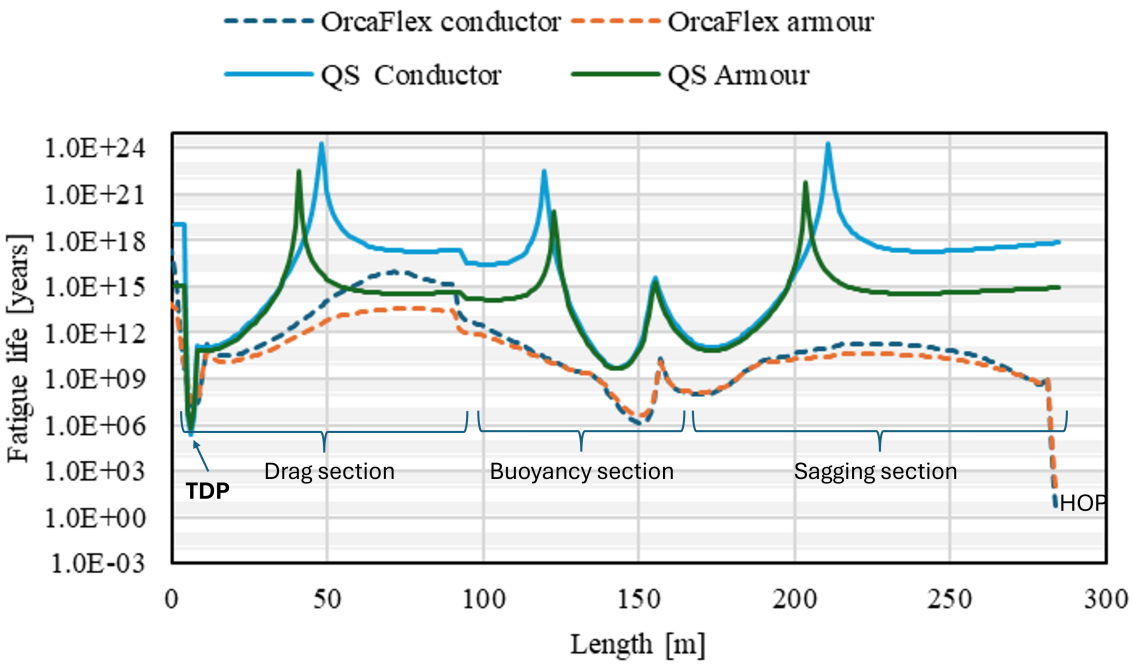

Figure 33: Fatigue life comparison between QS and FEM models

5. POWER CABLE DESIGN

This section covers the design and analysis of a power cable using OrcaFlex, applying the methodology discussed in **Chapter 3**. The chapter starts by outlining the prerequisites for analyzing a DPC in OrcaFlex and then details the properties necessary to model the cable. It includes an analysis of three initial proposed configurations to determine the distribution of curvature and effective tension, followed by the use of an optimization algorithm to enhance the cable configuration. Finally, both the initial and optimized configurations are evaluated for fatigue, and a new configuration is suggested based on the findings.

5.1. OrcaFlex setup

OrcaFlex is an advanced software application designed for the dynamic analysis of offshore marine systems. It is widely used in the oil and gas sector, in the field of renewable energy, and by marine engineers to simulate and study the performance of different marine structures under varying environmental conditions. This dynamic analysis tool specifically caters to offshore marine systems, utilizing numerical techniques to address the equations of motion for various marine structures in various environmental scenarios.

Instead of addressing the cable and the FWT as a combined system, the motion of the platform is initially estimated under specific environmental conditions. The next step involves creating a new model that includes only the cable and the platform, the environmental conditions remain the same as for the full FWT model, but the platform's motion is prescribed by the results from step 1.

5.1.1. General data

The general class object contains information related to the model configuration.

- The static analysis is solved in two phases, first by solving the equilibrium equations for each component, then by solving the coupled system.
- The methods used in the dynamic analysis, its convergence criteria, and damping factors to have a stable solution.
- The simulation is divided into stages to manage different phases of the analysis effectively; build-up, simulation, and operational sequences.

5.1.2. Environmental data

The environment class object refers to the properties necessary to represent the environment where the structures are supposed to operate.

- The properties required to characterize the sea include the kinematic viscosity ($1.35 \times 10^{-6}\ m^2/s$), the density of the water ($1.025\ t/m^3$), the water depth (200 m) and the coordinate reference system.
- The wave direction is set to zero and the JONSWAP model is used for the wave spectrum, with a random seed (12345) and 200 frequencies generated to represent the wave spectrum.
- The current direction is set to zero, and the maximum current is obtained from the STSS data.
- The wind direction is set to zero and its value is derived from STSS data.

5.2. Cable modeling

DPCs are engineered to endure intense cyclical stress, the mooring lines produce the horizontal tension necessary to control the platform offset, DPs must have enough cable to not enter in tension when the platform undergoes its maximum offset. Because the stress in the cables depends on the effective tension and curvature, the load varies along the cables, in consequence the damage along the cable differs in each segment; for example in at the HOP the damage is larger than any other section, because in this section the curvature and tension are maximum. Manufacturers set safe operational constraints to maintain the cable's longevity during its operational life.

In normal operation, the platform moves around its equilibrium position; therefore, ensuring an initial DPC configuration with low tension and curvature distribution reduces the stresses in the cable during operation.

The cable (see Fig. 34) has its endA fixed on the platform at (0, 0, -14), this part transmits the motion of the platform to the cable. On the other hand, endB is fixed in the seabed (AP); section 1 represents the sagging part, section 2 denotes the buoyancy part, and section 3 indicates the drag part. The buoyancy modules listed in (Tab. 11) are placed at intervals of 2 [m].
The entire cable employs the same type of line (Tab. 10), and to construct the buoyancy section, the floaters are introduced as attachments that provide additional buoyancy, thereby forming the lazy wave profile.

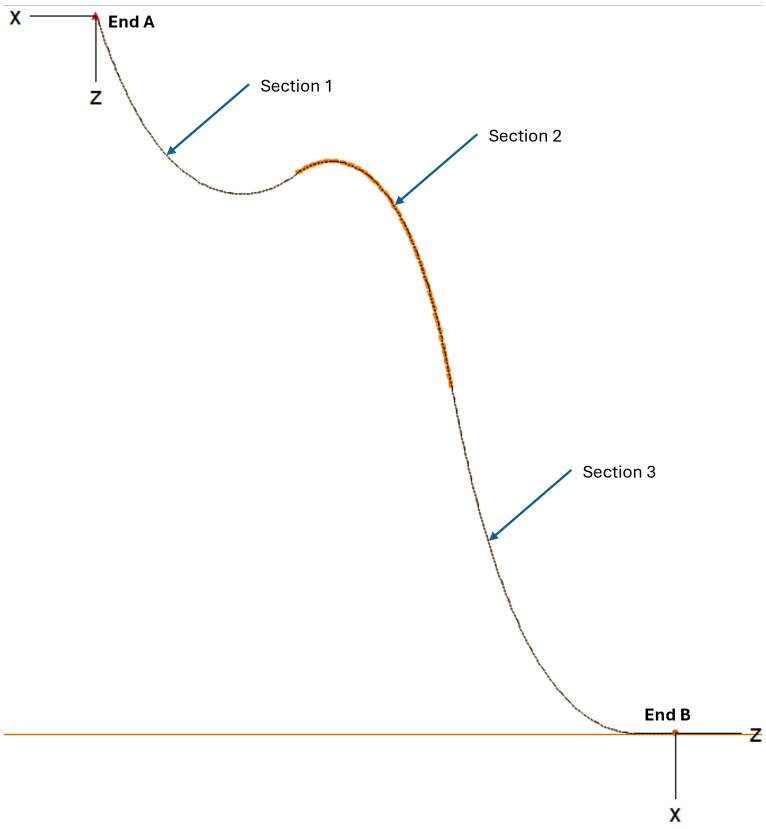

Figure 34: Local coordinate system for DPC modeling in OrcaFlex.

Table 10: Line properties

Parameter	Dimension	Value
Weight	kN/m	0.245
Buoyancy	kN/m	0.106
Submerged weight	kN/m	0.139
Mass	t/m	0.025
Displaced mass	t/m	0.011
Submerged mass	t/m	0.014
Diameter to submerged weigth ratio	m/(kN/m)	0.835
Diameter to submerged mass ratio	m/(t/m)	8.188

Table 11: Floater properties.

Parameter	Dimension	Value
Weight	kN	0.427
Buoyancy	kN	1.134
Submerged weight	kN	-0.707
Mass	Kg	44.0
Displaced mass	Kg	11.6
Submerged mass	Kg	-72.0

5.2.1. Configurations

In addition to the motion of the HOP caused by the movement of the platform, the current is also taken into account. Typically, the current velocity decreases with depth (see Fig. 35) starting from the water surface, the higher the velocity the more it influences the cable's motion.

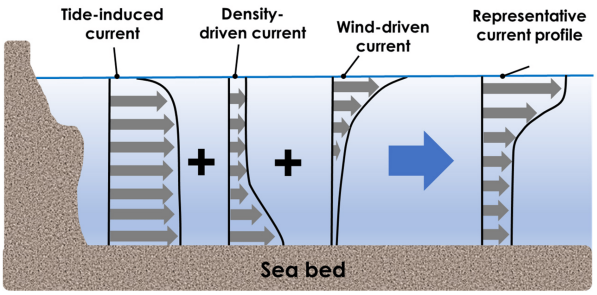

Figure 35: Schematic representation of the current profile [16].

Different configurations (see Fig. 36) are established to study the impact of the placements of the floaters on the initial curvature and effective tension, the vertical distance from the HOP to the ocean floor (D) measures 186 meters, while the horizontal distance from the vertical line of the HOP to the AP (L) is 150 meters. All configurations have the line type (Teb. 10) and floaters (Tab. 11).

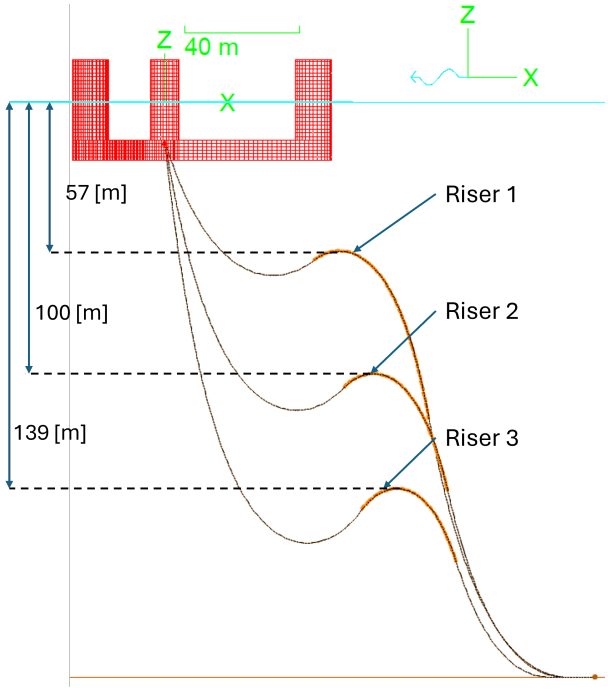

Figure 36: DPC initial configurations.

The Riser1 configuration is subject to higher current speeds because of the larger area

concentrated in the upper part of the cable where the current speed is higher (see Fig. 35), the Riser2 configuration is less affected by the current speed but increases the tension at the HOP, finally, the Riser3 configuration is less affected by the current speed profile but has the higher tension at the HOP.

The cable comprises three sections (Tab. 12), each section is segmented into one-meter length elements. In highly stressed areas, it is recommended to reduce the segment size [20], as OrcaFlex evaluates the cables using a finite lumped mass element method. For example, at the HOP and the touchdown point, a smaller segment will offer more detailed information on the occurrences at these specific locations. Given that this study aims to investigate the dynamic response of the cable relative to the vertical position of the floaters, segments of one meter are enough to describe it.

The buoyancy segment can be simulated in a couple of ways. First, by treating the buoyancy segment as a distributed cable, it is necessary to establish a new line type, which should encapsulate the attributes of both the basic cable and the buoyancy modules. The second alternative approach is to position the floaters along the buoyancy section, ensuring that the position of each floater corresponds to a cable node.

The floaters are located along the length of the cable, its 1D local reference system starts at endA and ends at endB (see Fig. 34), the initial and final positions of the floaters for each setup are displayed in (Tab. 13), and they are positioned every two meters along the buoyancy section. The quantity of floaters differs between riser systems; adding more floaters elevates the buoyancy section, whereas fewer floaters bring it down. In the absence of floaters, the cable arrangement forms a simple catenary profile.

Table 12: Initial cable configurations.

Riser	**Section length [m]**
Riser 1 -section 1	79.45
Riser 1 -section 2	77.46
Riser 1 -section 3	119.7
Riser 2 -section 1	129.45
Riser 2 -section 2	60.68
Riser 2 -section 3	93.77
Riser 3 -section 1	179.45
Riser 3 -section 2	46.99
Riser 3 -section 3	72.61

Table 13: Initial floaters distribution.

Parameters	Riser 1	Riser 2	Riser 3
Start from HOP [m]	79.45	129.45	179.45
End from HOP [m]	157.45	191.45	227.45
Number of floaters	40	32	25

5.3. Static analysis

5.3.1. Stress estimation

Riser1 has the lowest effective tension at the HOP (see Fig. 37),however, its curvature in the buoyancy section is higher than the other configurations. However, the combination of curvature and effective tension in the buoyancy section results in the highest static stress (see Fig. 38) for both the conductor and the armour.

Once the effective tension and curvature are determined, the stress is computed using the stress factor method. The armour experience higher stress than the conductor component (see Fig. 38), since the curvature stress factor is greater than the tension stress factor the higher stress points are located where the curvature is maximum.

The stress distribution also indicates increased stress concentrations in the HOP (left side of figure 38), attributed to the higher curvature in this segment because it has to reach perpendicular to the platform. The analysis of this event is beyond the scope of this thesis; typically, bending stiffeners are used to mitigate this issue.

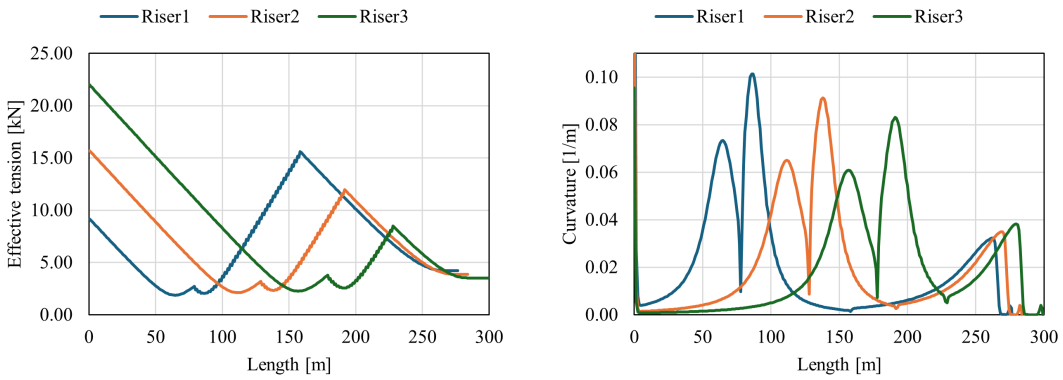

(a) Effective tension. **(b)** Curvature.

Figure 37: Initial DPCs configuration: curvature and effective tension.

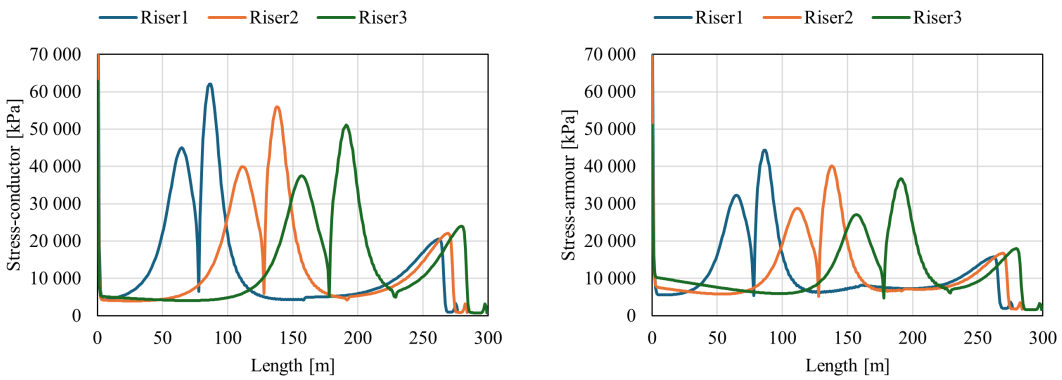

(a) Conductor stress. **(b)** Armour stress.

Figure 38: Initial DPCs configuration: conductor and armour stresses.

5.3.2. Optimization results

The weight function associates a value for the initial configuration, then the algorithm runs to minimize the function by applying a simple step descent method, it stops when a certain optimization ratio or number of iterations is achieved. In this study, the algorithm terminates when it reaches 10% optimization of its starting value or completes 100 iterations (see Sect. 3.5.1).

The weight function introduced in Sec. 3.5.1 is implemented for the three initial configurations; the maximum allowed curvature is set to 0.566 $[1/m]$, the minimum curvature necessary to decouple motion from the platform is 0.15 $[1/m]$, and the maximum effective tension allowed for safe operation is 885 $[KN]$ (see Tab. 4) and finally a reference length of 300 $[m]$ is considered to run the optimization algorithm. The optimized cable configurations are listed in (Tab. 14), and its profiles are presented in (Fig. 39).

The curvature and effective tension of the three configurations are shown in (Figs.40-42). At first sight, it is evident that the cable has achieved a smooth profile throughout its entire length from the HOP to the TDP.

The effective tension distribution has two maximums; the first maximum is located at the hang-off point and holds the majority of the sagging section, and this value does not appear to be influenced by the optimization since the operational tension recommended by the manufacturers is significantly higher than the actual tension. The second maximum is found at the end of the buoyancy segment and mainly supports the weight coming from the drag section; this can be greater or smaller than the tension at the hang-off point depending on the vertical distribution of the buoyancy modules.

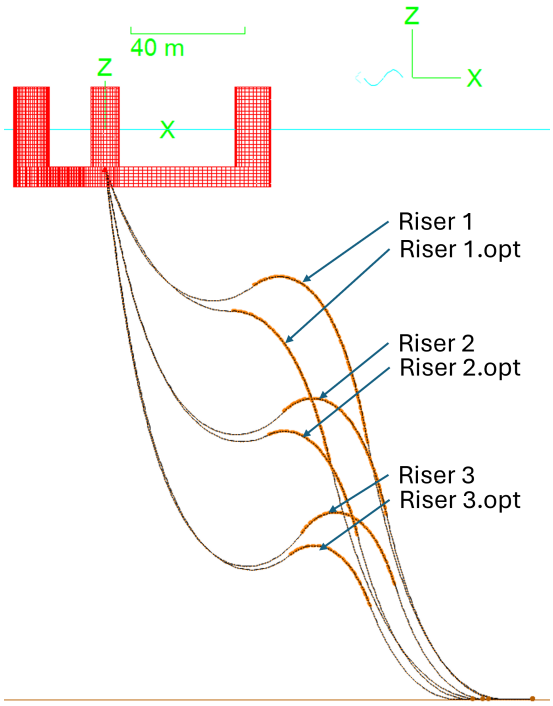

Figure 39: Initial and optimized profiles of cables.

Table 14: Initial and optimized cables´s configuration.

Parameter	Initial	Optimized
Riser 1 -section 1 [m]	79.45	71.80
Riser 1 -section 2 [m]	77.46	69.81
Riser 1 -section 3 [m]	119.70	104.09
Anchor point(AP) [m]	150	134.39
Nº floaters	**40**	**34**
total length [m]	**276.61**	**245.70**
Riser 2 -section 1 [m]	129.45	123.70
Riser 2 -section 2 [m]	60.68	54.93
Riser 2 -section 3 [m]	93.77	76.24
Anchor point(AP) [m]	150	132.47
Nº floaters	**32**	**27**
total length [m]	**283.90**	**254.87**
Riser 3 -section 1 [m]	179.45	172.84
Riser 3 -section 2 [m]	46.99	40.38
Riser 3 -section 3 [m]	72.61	51.37
Anchor point(AP) [m]	150	128.76
Nº floaters	**25**	**20**
total length [m]	**299.05**	**264.58**

The second maximum of the effective tension distribution had moved to the left side (Figs. 40-42 (a)) after the optimization process, as a result of the shortening length of the sagging section.

The curvature distribution has four maximum values; the highest occurs at the HOP, the second maximum is located at the lowest point of the sagging segment, the third one is located at the highest point of the buoyant segment, and finally a local maximum is also found at the TDP (Fig. 30 (b)). After the optimization process, new configurations are formed, resulting in decreased maximum values located at the respective peaks (see Figs. 40-42 (b)).

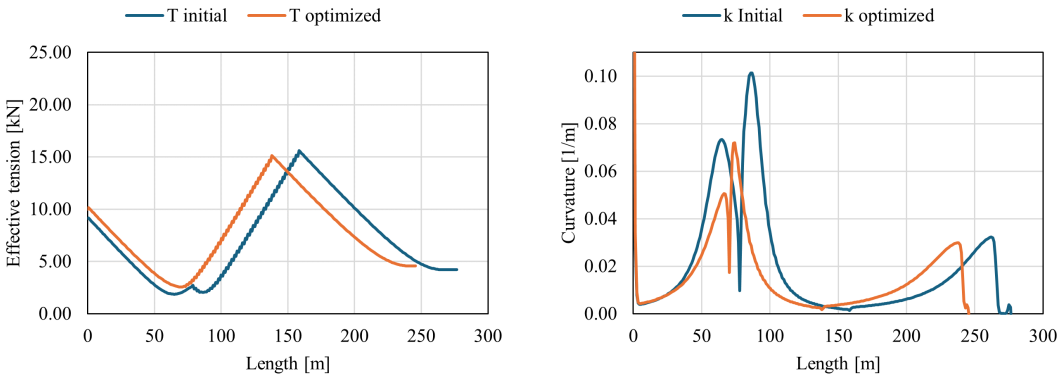

(a) Effective tension. **(b)** Curvature.

Figure 40: Results for initial and optimized Riser 1 conditions.

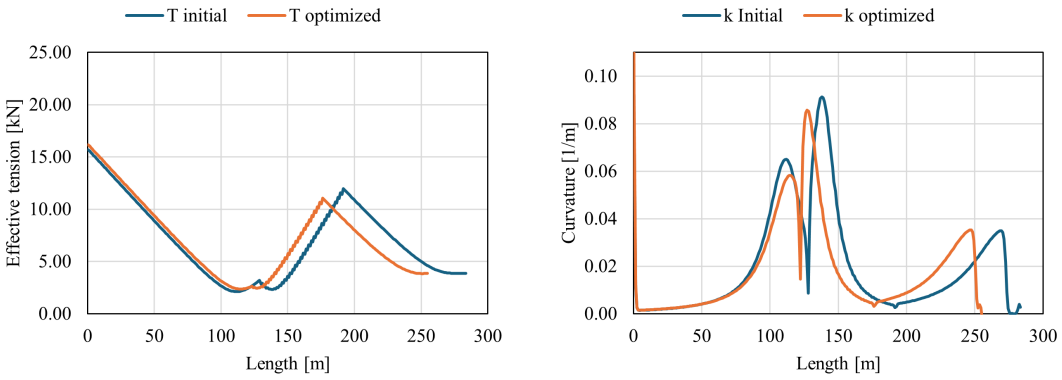

(a) Effective tension. **(b)** Curvature.

Figure 41: Results for initial and optimized Riser 2 conditions.

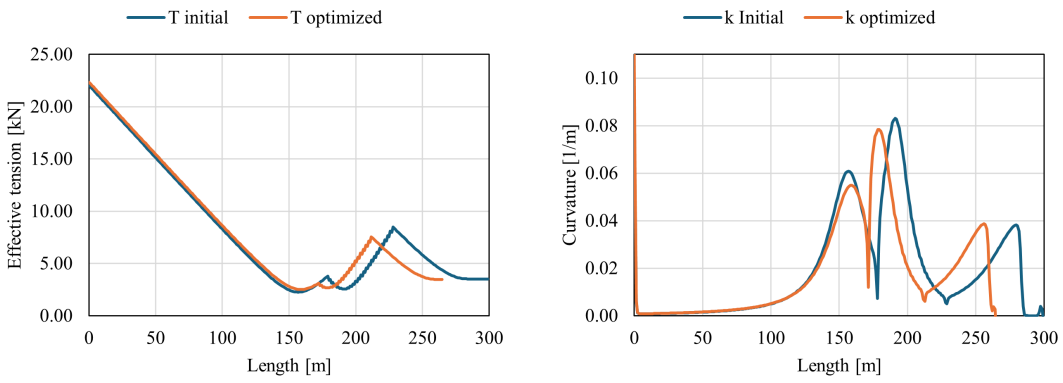

(a) Effective tension. **(b)** Curvature.

Figure 42: Results for initial and optimized Riser 1 conditions.

5.4. Fatigue analysis

According to the explanation provided in Sect. 3.6, the damage assessment is performed for all six DPC configurations. The dynamic simulation is divided into two stages: the first stage lasts for 420 seconds and the second stage lasts for 30 minutes. Subsequently, to compute the damage, the duration of each STSS, as listed in Table 5, is calculated by multiplying its probability of occurrence by the total number of hours in a year (8 760 hours).

The fatigue analysis is estimated in OrcaFlex, this is a post-processing tool that requires as inputs; dynamic simulation of all STSS, mechanical properties of the cables, S-N fatigue curves of the components, and stress factors. More details are included in (App. B.1).

5.4.1. S-N curves

The S-N curves are introduced in OrcaFlex as tabular data for both the steel armour and copper conductor. Initially, the fatigue characteristics of the conductor are depicted using ϵ-N, then, assuming that the material does not experience plastic deformation, the curve S-N (Fig. 43) is derived simply by multiplying the strain (ϵ) by its Young modulus (E).

5.4.2. Cable´s life estimation

For the optimized Riser1 (see Fig. 42), the small final curvature along the sagging section negatively impacts the decoupling of motion and cannot endure greater excursions. This is because its short length leads to increased tension in the cable. In this specific case, most of the stress originates from effective tension. The optimization algorithm found an optimal configuration to reduce the effective tension, curvature, and length of the cable

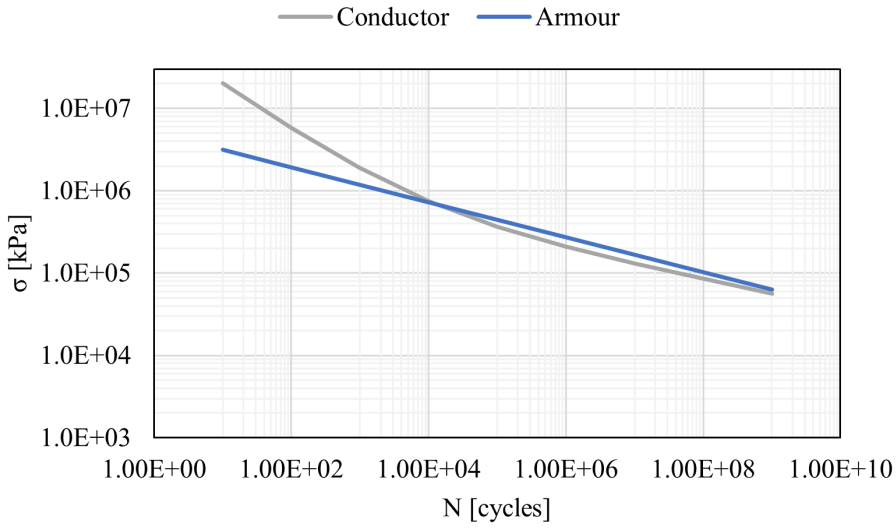

Figure 43: S-N Curves for conductor and armour.

when the platform is not moving. However, the optimized configuration fails in dynamic analysis, and consequently, this configuration has a very short life (curves Conductor.opt and Armour.opt Fig. 44).

This highlights the importance of giving the cable enough initial curvature in the sagging section to allow the system to not be in tension when the platform moves. With this premise, the system is divided into two sections; Only the weight of the sagging section (section 1) is transferred to the HOP, while the drag section (section 2) is suspended in the buoyancy section (Fig. 34).

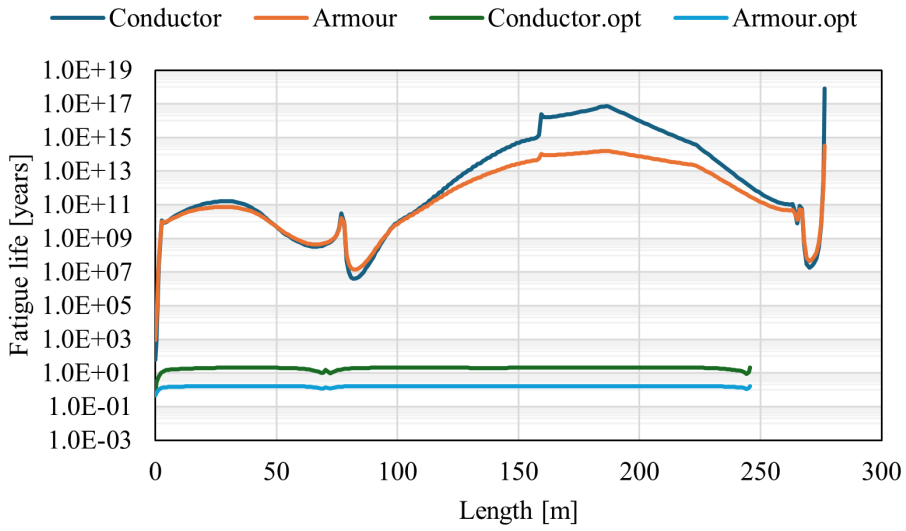

Figure 44: Fatigue life estimation for Riser 1 and its optimized version.

The optimized Riser2 configuration reduces tension in the HOP and curvature in the sagging and buoyancy section, but similar to the Riser1.opt there is a big reduction in the curvature in the sagging section (see Fig. 39). This has a detrimental effect on the system by raising the tension at the HOP during platform movements. However, while damage in the TDP is mitigated, damage in the HOP has increased, leading to a reduction of 7 years in its fatigue life (see Tab. 15).

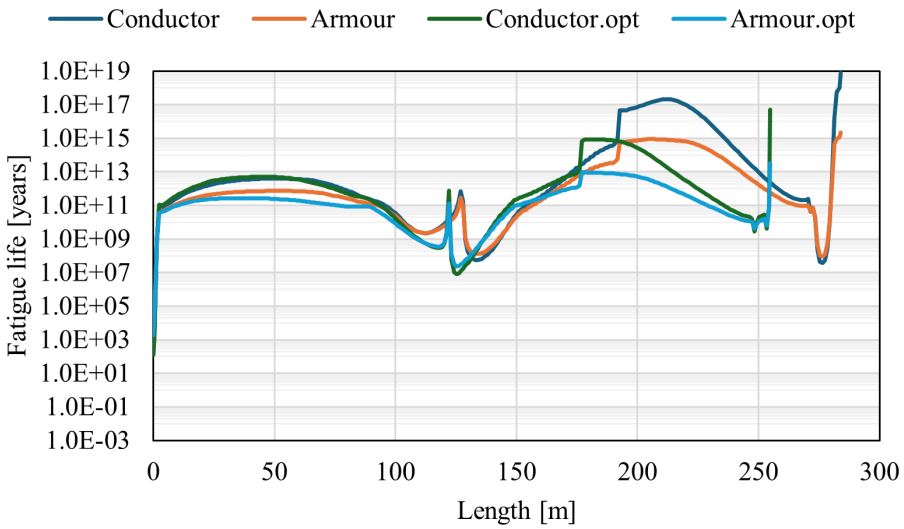

Figure 45: Fatigue life estimation for Riser 2 and its optimized version.

The Riser3 optimized configuration has given positive results by increasing the cable life by 15 years, although the life at the top of the buoyancy section has been reduced (see Fig. 46). This suggests that even increasing the tension at the HOP, the cable performs better in fatigue.

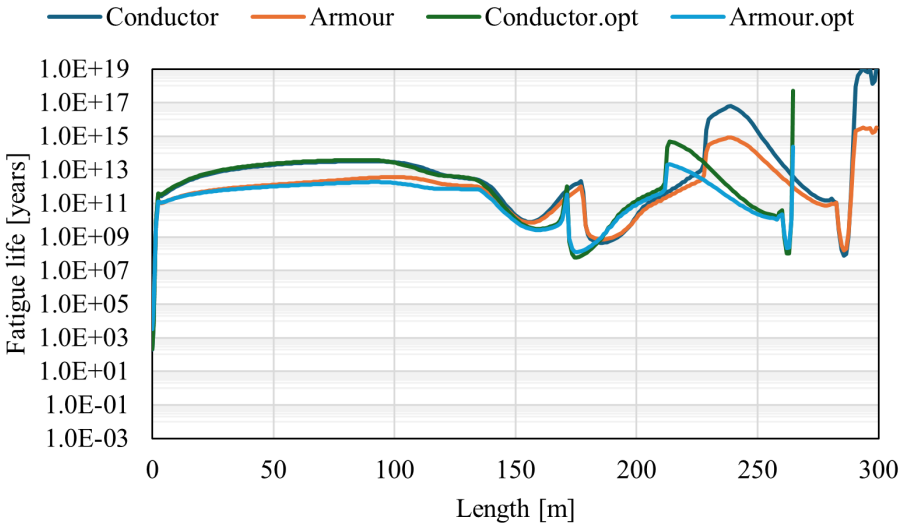

Figure 46: Fatigue life estimation for Riser 3 and its optimized version.

Although optimized configurations require less cable length and floaters, they do not always increase the lifespan of the cable (Tab. 15). For example, the lifespan of Riser2 decreases from 127 years to 120 years at the HOP, in contrast to Riser3, which increases from 195 years to 210 years. In both scenarios, the main critical component is the conductor.

Table 15: Life span at the HOP in years.

Condition	Riser1	Riser2	Riser3
Initial	58	127	195
Optimized	1	120	210

All configurations have lifetimes exceeding 32 years, except Riser1.opt (Tab. 15). Another factor to consider when choosing the best candidate could be the amount of material required for their construction (Tab. 14).

The optimal lazy-wave configuration appears to be the one with the floaters positioned as close to the bottom as feasible. The advantages of this setup include the following.

- Even though it has more hanging cable, it performs as good as the other configurations. The increase in the HOP does not have a significant effect in the life of the cable.
- The fatigue life does not seem to be affected by the increase of hanging section; in fact, configuration Riser2 and Riser3 have a fatigue life more than 100 years at the HOP, compared to the only 32 years required for operational life service.
- Less floaters are needed to make a lazy wave configuration.
- Marine growth at the sea bottom is less aggressive than near the surface. In consequence, the decoupling produced by the floaters will last longer.

5.5. Novel proposal

The study suggests a new configuration (Riser 4) based on the analysis discussed above. This could be the most cost-effective lazy wave system (Fig. 47). This consists of a larger sagging section that hangs vertically at the HOP, a small buoyancy section that is just enough to decouple motion from the HOP to the TDP, and a drag section that is sufficient to allow the platform to develop its maximum excursion without putting the cable in direct tension.

The modified configuration exhibits an increased initial curvature due to the shorter lengths of the hogging and sagging humps; subsequently, the optimization algorithm is used to enhance the configuration of the DPC. The optimized configuration (Riser 4.opt) produces a smaller tension at the HOP and the curvature in the sagging section and the buoyancy section is reduced as well. The configuration is shown in (Fig. 47).

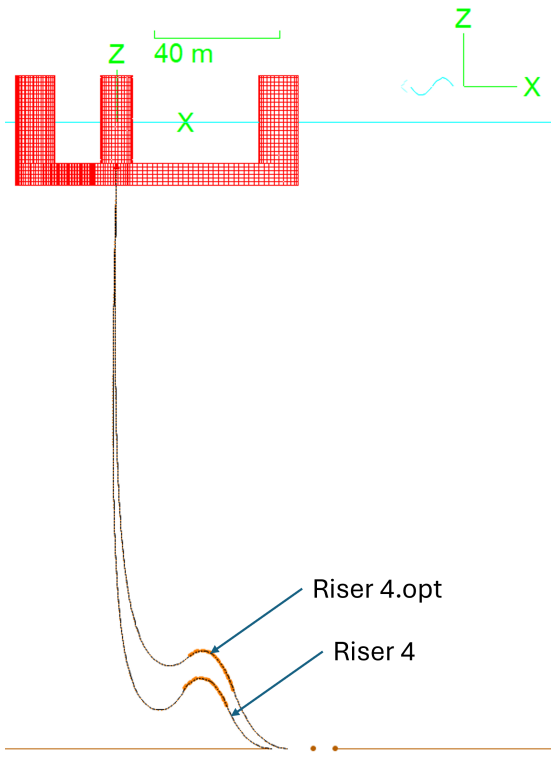

Figure 47: Fatigue life estimation for Riser4 and ant its optimized version.

The configuration meets the minimum fatigue life requirements of 32 years (see Tab. 17) and is the cheapest, it requires just 229 meters of cable and 11 floaters for construction, compared to the 10 floaters and 250 meters of the original setup (see Tab. 16).

The fatigue life of this new configuration has been reduced by 10 years at the HOP, but there is no significant variation in the rest of the cable (Fig. 48). Alternative configurations

Table 16: Initial and optimized configuration for Riser 4.

Parameter	Initial	Optimized
Riser 4 - section 1 [m]	180.00	173.00
Riser 4 - section 2 [m]	30.00	23.00
Riser 4 - section 3 [m]	40.00	33.00
Anchor point (AP) [m]	70.0	63.0
Number of floaters	**10**	**11**
Total length [m]	**250.00**	**229.00**

Table 17: Life span at the HOP for Riser 4 configuration.

Condition	Life in years
Initial	195
Optimized	185

could be tested to enhance the DPC. For instance, positioning the AP closer to the vertical line of the HOP requires less cable to generate the same curvature in the hump of the sagging section, to decouple motion from platform to affect the TDP.

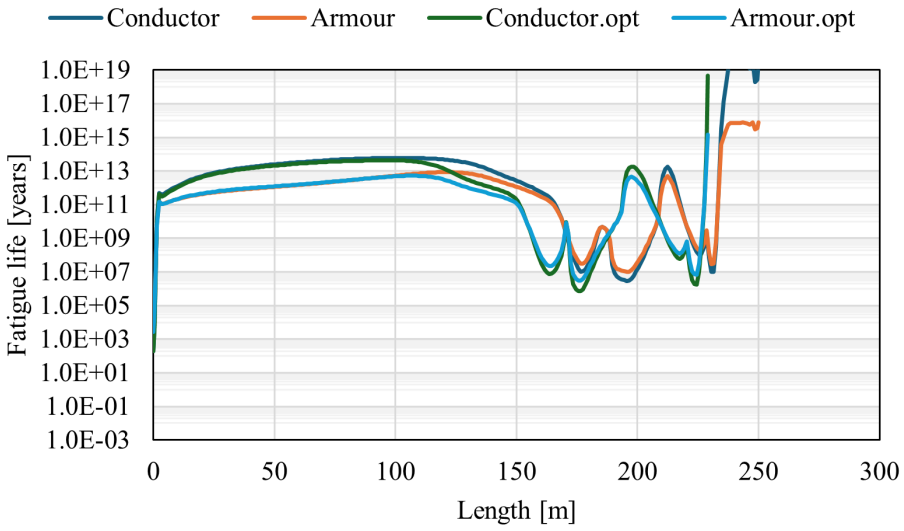

Figure 48: Fatigue life of Riser 4.

5.5.1. Extreme analysis

The curvature and the effective tension are analyzed during the extreme loading condition, these values are compared with the recommended operating values given by the manufacturers. As a reference, the values for the installation/deployment of the curvature and effective tension are 0.625 [1 / m] for the curvature and 182.56 [KN], respectively [12].

Based on the distribution of the annual maximum significant wave height [9], a sea state

(storm) is estimated to last 3 [h]. To represent this extreme event, the values form (Tab. 6) are considered. During this period, the findings are as follows: the curvature (Fig. 49) reaches a maximum of 0.43 [1/m], a minimum of 6.68e-04 [1/m], and an average value of 0.1655 [1/m]. On the other hand, for effective tension (Fig. 50), the highest recorded value is 90.61 [KN], the lowest is 22.49 [KN], and the average value is 28.12 [KN].

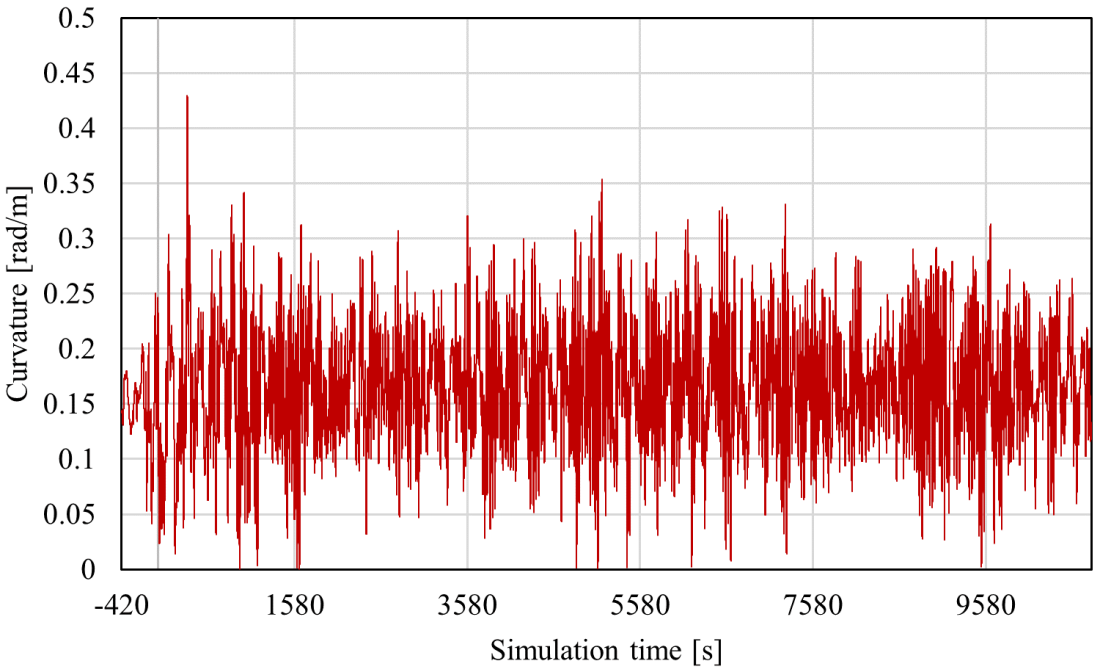

Figure 49: Curvature at the HOP under extreme loading condition.

5.5.2. ULS

The **ultimate limit state (ULS)** refers to the maximum loads or forces that a structure can withstand without collapsing or experiencing irreversible damage. Essentially, respecting this limit ensures that the structure remains safe and functional even under severe conditions. For the DPC it refers to the tension that the cable can withstand under safe operating conditions, and it should be noted that the tension must be smaller than that at which the conductor yields. From this reference value (see Tab. 4), the maximum allowed tension (Eq. 59) can be estimated considering a material safety factor (γ_m) and a load safety factor (γ_f), According to the suggested guidelines for subsea power cables in shallow water [8], these values generally fall between 1.3 and 1.5 for the material safety factor and between 1.3 and 1.6 for the load safety factor.

$$T_{allowed} = \frac{ULS_{cable}}{\gamma_m \cdot \gamma_f} \tag{59}$$

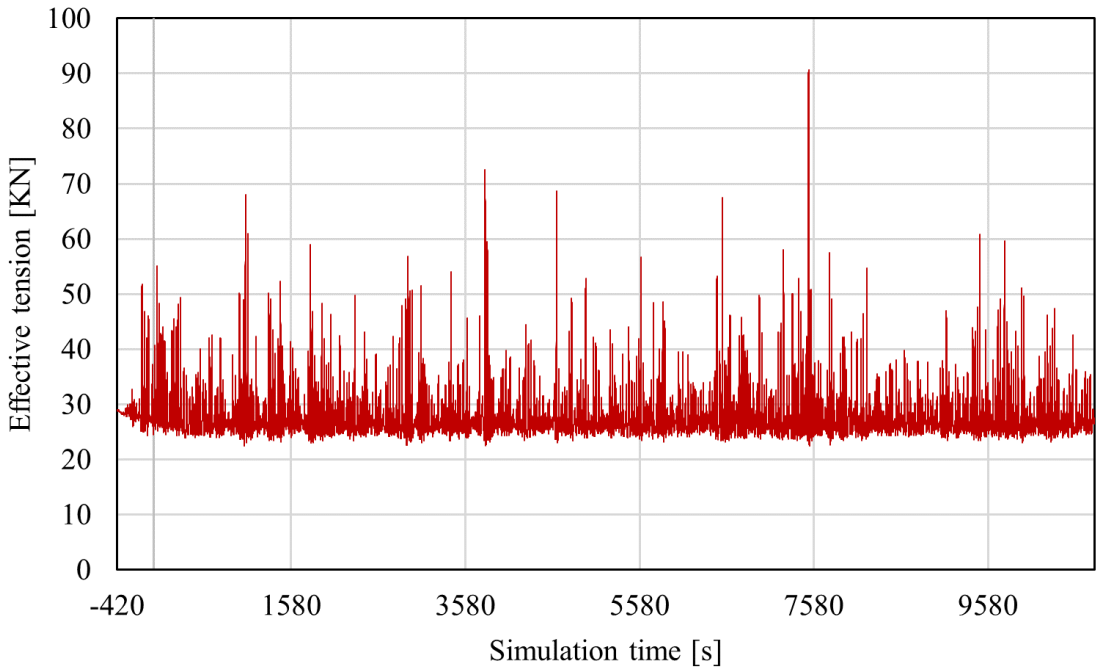

Figure 50: Effective tension at the HOP under extreme loading condition.

$$T_{allowed} = \frac{885[KN]}{1.4 * 1.6}$$
$$T_{allowed} = 421.43[KN]$$

The cable satisfies this ULS, the maximum tension estimated in the extreme loading cases is 90.61 [KN] far below the maximum allowed tension.

6. CONCLUSIONS

6.1. Short term sea state

The environmental conditions to perform a fatigue analysis of the DPC are estimated using a simplified join probability function [19] (see Chapter 3). The inputs; PDF for wind speed and the scatter diagram for wave characterization are both taken from *Puertos del estado*, for the buoy *Villano Sisaras*. The parameters for the join probability function are given in an analysis [19] of the data register by the buoy *Cabo Silleiro*.

6.2. Quasi static model

The quasi-static model described in **Chapter 4** can be utilized to address the lazy wave issue, offering a precise configuration of the DPC shape. Despite the omission of the bending and torsional stiffness of the model in its formulas, it achieves a smaller maximum deviation than 1% along the cable, compared to the complete model set-up in OrcaFlex. This model is also suitable for an initial analysis of the effective curvature and tension distribution, the curvature of the cable is well represented with the exception of the HOP. On the other hand, the effective tension estimated with this method can be used with confidence along all the length of the DPC.

The algorithm designed to address the QS problem is tailored for the lazy wave configuration. However, once the platform's excursion is determined, it is recommended to concentrate on resolving the system solely at the peaks and troughs of the data. Since the rain flow counting method considers only these points, this approach is efficient in calculating damage, as it reduces the number of computations.

6.3. Power cable design

The best configuration seems to be when the buoyant hump is located as low as possible, requiring less of the cable length and floaters. With this configuration, the stress at the HOP comes mainly from the effective tension because the he curvature is small. It is also important to note that at this position, the buoyancy of the floaters could last longer as less marine growth is expected.

The optimization algorithm is designed to improve the configuration of the lazy wave riser system by reducing the tension at the HOP, the curvature along the cable, and the total length. However, the algorithm only takes into account static performance; therefore,

it is recommended to verify whether this new configuration satisfies the required fatigue life.

For fatigue assessment, the dynamic reaction of DPC to each STSS is evaluated, and damage is calculated based on the likelihood of encountering that load condition (see Tab. 5). As a result, the majority of configurations examined in this section meet the minimum design life requirement of 32 years, with the exception of one configuration. This particular configuration, with the smallest initial curvature in the sagging section, causes the DPC to experience significant axial tension as soon as the platform starts to move horizontally.

Although there are advantages such as an increased fatigue life and a reduced need for cable length and floaters in construction, positioning the buoyancy hump close to the seabed complicates the repair process when the cable flails. A longer portion of the cable will be affected by a failure at the HOP due to the increased tension in the sagging sections, and the use of advanced remotely operated vehicles is required to retrieve the cable's end.

6.4. Future Work

- Assess the minimum permissible height between the lowest point of the sagging section and the seabed.
- Examine the correlation between the laying length and the maximum excursion of the platform.
- Evaluate the minimum required buoyancy length to isolate the platform's motion from the touch down point.
- Evaluate the performance of the cable by adding bend stiffeners at the HOP and TDP.
- Model the DPC including all the ancillary equipment. Calculate the fatigue life and assess the expenses associated with these updated configurations.

References

[1] Christopher Allen, Anthony Viscelli, Habib Dagher, Andrew Goupee, Evan Gaertner, Nikhar Abbas, Matthew Hall, and Garrett Barter. *Definition of the UMaine VolturnUS-S reference platform developed for the IEA wind 15-megawatt offshore reference wind turbine*. Tech. rep. National Renewable Energy Lab.(NREL), Golden, CO (United States); Univ. of ..., 2020.

[2] Global Wind Atlas. *Global Wind Atlas - Spain*. Accessed: 2024-08-07. 2024. URL: https://globalwindatlas.info/en/area/Spain.

[3] Dennis Beier, Anja Schnepf, Sean Van Steel, Naiquan Ye, and Muk Chen Ong. "Fatigue Analysis of Inter-Array Power Cables between Two Floating Offshore Wind Turbines Including a Simplified Method to Estimate Stress Factors". In: *Journal of Marine Science and Engineering* 11.6 (2023), p. 1254.

[4] Daniela Benites-Munoz, Pierpaolo Ricci, Imanol Touzon, Fernando Salcedo, Rupert Raymond, and Diogo Nunes. "Fatigue-life prediction methods of a dynamic power cable for a floating testing platform–a numerical approach". In: *Proceedings of the European Wave and Tidal Energy Conference*. Vol. 15. 2023.

[5] Adam J Collin, Anup J Nambiar, David Bould, Ben Whitby, MA Moonem, Benjamin Schenkman, Stanley Atcitty, Paulo Chainho, and Aristides E Kiprakis. "Electrical components for marine renewable energy arrays: A techno-economic review". In: *Energies* 10.12 (2017), p. 1973.

[6] Wikipedia contributors. *Curvature*. https://en.wikipedia.org/wiki/Curvature. Accessed: 2024-07-19. 2024.

[7] DNV. *RECOMMENDED PRACTICE DNV-RP-C203, Fatigue design of offshore steel structures*. Ed. by DNV. DNV, 2021.

[8] DNV GL. *Subsea power cables in shallow water*. Edition: Mar, 2016 (Oct, 2021). Mar. 2016. URL: https://standards.dnv.com/explorer/document/59D1E3B7C7A14A4DB2F8A2E53F152.

[9] *Environmental conditions and environmental loads DNV-RP-C205*. 2021.

[10] U.S. Department of Energy. *Offshore Wind Energy Strategies*. Tech. rep. Accessed: 2024-08-21. Washington, DC: U.S. Department of Energy, Jan. 2022. URL: https://www.energy.gov/sites/default/files/2022-01/offshore-wind-energy-strategies-report-january-2022.pdf.

[11] Wind Europe. *Wind Energy in Europe 2023: Statistics and the Outlook for 2024-2030*. Accessed: 2024-08-07. 2023. URL: https://windeurope.org/intelligence-platform/product/wind-energy-in-europe-2023-statistics-and-the-outlook-for-2024-2030/.

[12] Theodor Didriksen Hansen. "Utsira Nord Floating Wind farm – Optimalisation of marine operations related to inter-array cable installation". Accessed: 2024-08-12. Master's thesis. University of Stavanger, 2023. URL: https://uis.brage.unit.no/uis-xmlui/bitstream/handle/11250/3089217/no.uis%3ainspera%3a129711464%3a35882929.pdf?sequence=1.

[13] Qusay Hassan, Patrik Viktor, Tariq J Al-Musawi, Bashar Mahmood Ali, Sameer Algburi, Haitham M Alzoubi, Ali Khudhair Al-Jiboory, Aws Zuhair Sameen, Hayder M Salman, and Marek Jaszczur. "The renewable energy role in the global energy Transformations". In: *Renewable Energy Focus* 48 (2024), p. 100545.

[14] IBM. *A Brief History of Renewable Energy*. Accessed: 2024-08-21. 2024. URL: https://www.ibm.com/blog/renewable-energy-history/.

[15] M Ikhennicheu, M Lynch, S Doole, F Borisade, F Wendt, MA Schwarzkopf, M Denis, L Ramirez, and S Potestio. *Corewind D3. 1: Review of the state of the art of dynamic cable system design*. Tech. rep. Tech. rep., https://corewind. eu/wp-content/uploads/files/publications ..., 2020.

[16] Chan Ho Jeong, Min Kyu Ko, Moonjin Lee, and Seong Hyuk Lee. "CFD-Based Metamodeling of the Propagation Distribution of Styrene Spilled from a Ship". In: *Applied Sciences* 10.6 (2020), p. 2109.

[17] Stian Karlsen, Roger Slora, Kristian Heide, Sjur Lund, Fredrik Eggertsen, and Per Arne Osborg. "Dynamic deep water power cables". In: *Proceedings of the 9th International Conference and Exhibition for Oil and Gas Resources Development of the Russian Arctic and CIS Continental Shelf, RAO/CIS Offshore, St Petersburg, Russian*. Vol. 15. 2009.

[18] Stian Karlsen, Roger Slora, Kristian Heide, Sjur Lund, Fredrik Eggertsen, and Per Arne Osborg. "Dynamic deep water power cables". In: *Proceedings of the 9th International Conference and Exhibition for Oil and Gas Resources Development of the Russian Arctic and CIS Continental Shelf, RAO/CIS Offshore, St Petersburg, Russian*. Vol. 15. 2009.

[19] Lin Li, Zhen Gao, and Torgeir Moan. "Joint distribution of environmental condition at five european offshore sites for design of combined wind and wave energy devices". In: *Journal of Offshore Mechanics and Arctic Engineering* 137.3 (2015), p. 031901.

[20] Orcina Ltd. *Fatigue analysis*. https://www.orcina.com/webhelp/OrcaFlex/Content/html/Fatigueanalysis,Introduction.htm. Accessed: 10/07/2024. 2024.

[21] MARCO MASCIOLA and JASON JONKMAN. "Development of a multisegmented, quasi-static cable model with an analytical jacobian for modeling floating offshore wind turbines". In: (2013).

[22] MathWorks. *Rainflow Counting Algorithm*. Available online: https://es.mathworks.com/help/signal/ (accessed on June 28, 2024). 2024. URL: https://es.mathworks.com/help/signal/ref/rainflow.html.

[23] European Marine Observation and Data Network. *Map of the Week – Locations of Wind Farms*. European Marine Observation and Data Network (EMODnet). 2021. URL: https://emodnet.ec.europa.eu/en/map-week-locations-wind-farms-0.

[24] Puertos del Estado. *Oceanography - Puertos del Estado*. Accessed: 2024-08-08. 2024. URL: https://www.puertos.es/en-us/oceanografia/Pages/portus.aspx.

[25] Van Oord. *Van Oord*. Accessed: 2024-08-18. 2024. URL: https://www.vanoord.com/.

[26] WikiWaves. *Ocean-Wave Spectra*. https://wikiwaves.org/Ocean-Wave_Spectra. 2024.

[27] WindEurope. *Spanish Offshore Wind Reaches Key Milestone*. Accessed: 2024-08-21. 2024. URL: https://windeurope.org/newsroom/news/spanish-offshore-wind-reaches-key-milestone/#:~:text=WindEurope%20and%20the%20Spanish%20Wind%20Energy%20Association%20Asociaci%C3%B3n,hub%20for%20early%20offshore%20wind%20development%20in%20Spain..

[28] Shilun Zhao, Yongquan Cheng, Pengfei Chen, Yan Nie, and Ke Fan. "A comparison of two dynamic power cable configurations for a floating offshore wind turbine in shallow water". In: *AIP Advances* 11.3 (2021).

APPENDICES

A. Floater properties

Pipe Float

The PartnerPlast Pipe Float is a product designed to fit to hoses, wires and umbilicals. The Pipe Float consists of two half-cylindical buoyancy elements, and six distance- and friction blocks. The Roblon Quick Strap and tensioner fastens the complete module to the pipe/umbilical/wire. The pipe floats are available in all depth ratings from surface to 2500m. Standard color: bright yellow, optional: orange. Buoyancy figures are given seawater with density 1,025 kg/dm3. Weight figures are dry weight in air. Buoyancy figures are nominal net Buoyancy.

The Pipe Float has inner distance blocks in suitable thickness to fit the diameter of the customer's umbilical/pipe size. The blocks are made of Polyurethane shore 80A. The blocks are fitted and locked inside the PE half-cylindrical parts. Friction will keep the Pipe Float onto the umbilical/pipe. The Maximum hose/wire/pipe diameter is 250 mm. Although, any other smaller diameter for customer is available.

Main specifications

Depth	Buoyancy (kgf)	Weight (kg)
Surface	115,6	43,5
250 m	90,9	68,2
500 m	87,8	71,3

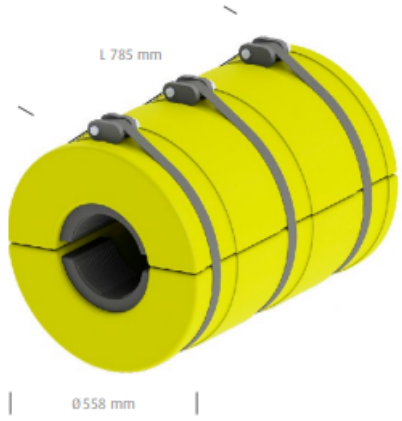

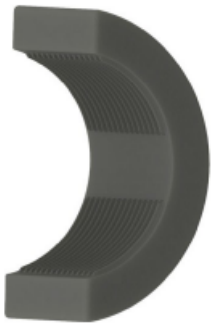

B. Weight function flow chart

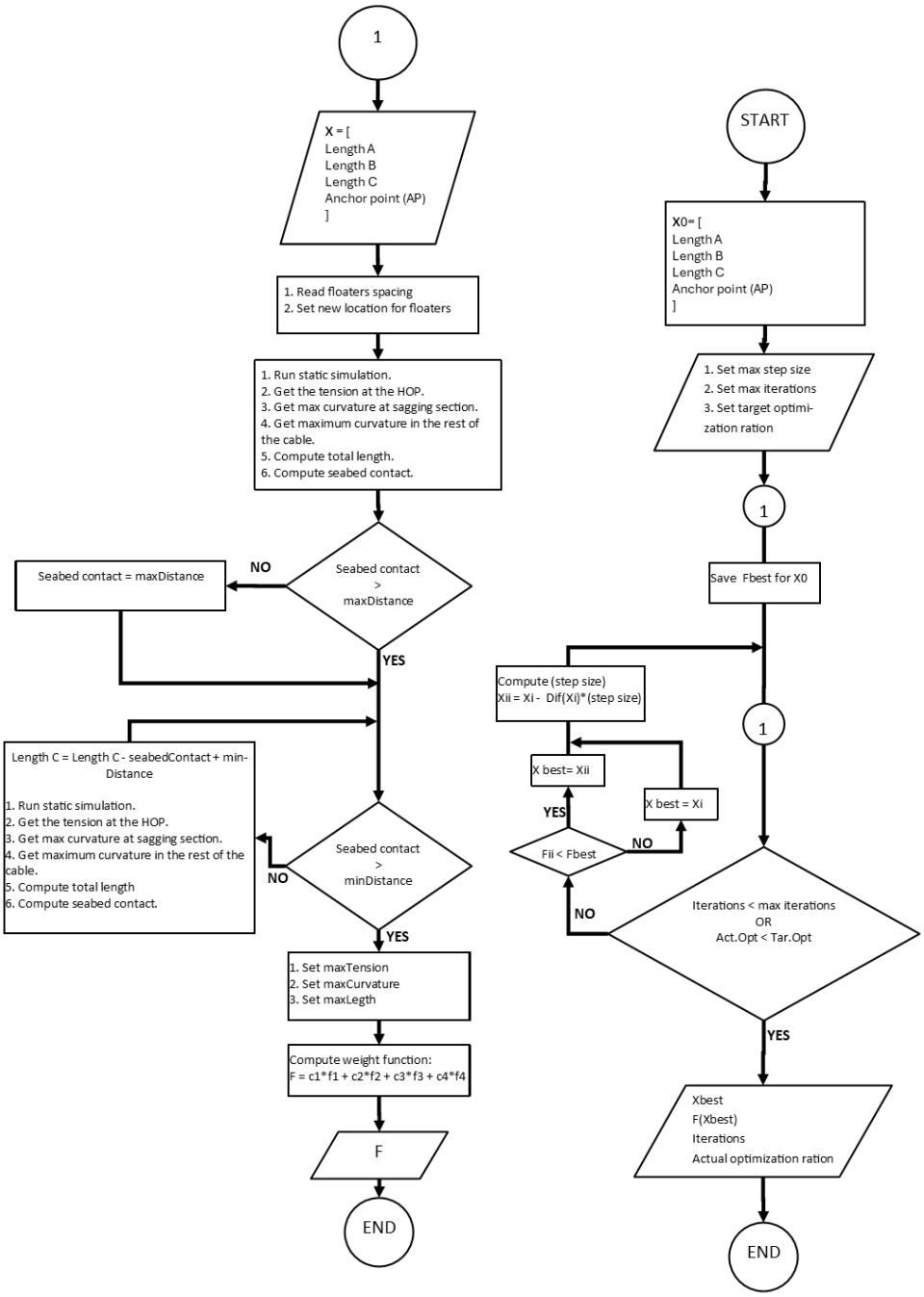

Figure 51: Weight function flow diagram

B.1. Fatigue analysis in OrcaFlex

The OrcaFlex fatigue analysis tool is a post-processor that calculates fatigue damage using a variety of methods. Fatigue damage is collated and summed for specified load cases and then presented in graphs or tables. The fatigue analysis tool is essentially a self-contained subprogram within OrcaFlex [20].

For umbilical cables, the stress recovery method employs stress factors, and damage is determined through deterministic irregular wave fatigue analysis using the rainflow cycle counting technique according to specified S-N curves. Here is a brief summary of the OrcaFlex recommendation[20].

B.1.1. Load cases

- Simulation file name: The name of the simulation file which represents the load case, either the full path or a relative path.
- Line name: The name of the line, in the load case simulation file, to be analysed(The line name will usually be the same in all load cases).
- Simulation period: The duration of the pre-run simulation file that specifies the load case. Generally, the initial segment of the simulation is discarded as stage 1, and the stable portion of the simulation is used for fatigue analysis.
- Duration of exposure: The cumulative time the system is subjected to this load case is calculated as $24h \cdot 365 \cdot P$, where P is the probability of the load case occurring as detailed in Tab. 5

B.1.2. Components

The elements under consideration are a copper conductor and steel armor wires. For the tension variable, the effective tension is chosen. The stress factors for each element are presented in (Tab.9), and the S-N curves can be found in Figures 18 and 17.

B.1.3. Analysis data

- Critical damage: This sets a warning level: if the total damage at any fatigue point exceeds this value, then that damage figure will be highlighted in the results. This facility is not available for histogram collation.
- Number of thetas: The number of points around the pipe circumference, at which fatigue analysis will be performed. There will be n of these fatigue points uniformly distributed at $360°/n$ intervals around the pipe circumference; by convention, the symbol θ (theta) is used to represent their circumferential position, hence the name

number of thetas. A larger number of thetas gives a more comprehensive analysis, but one which takes a little longer.

- Arc length intervals: You define the parts of the line to be analysed by specifying a number of arc length intervals in the form of from and to arc length values, z_{from} and z_{to} respectively. OrcaFlex will analyse cross sections at each line end and mid-segment whose arc length z is in the range $z_{from} \leq z < z_{to}$.For simple cases you can use just one arc length interval covering the whole line.